Modelling Electrochemical Energy Storage Devices in Insular Power Network Applications supported on Real Data

E.M.G. Rodrigues[a], R. Godina[a], J.P.S. Catalão [a,b,c,*]

[a] *C-MAST, University of Beira Interior, R. Fonte do Lameiro, 6201-001 Covilhã, Portugal*
[b] *INESC TEC and Faculty of Engineering of the University of Porto, R. Dr. Roberto Frias, 4200-465 Porto, Portugal*
[c] *INESC-ID, Instituto Superior Técnico, University of Lisbon, Av. Rovisco Pais, 1, 1049-001 Lisbon, Portugal*

Abstract

This paper addresses different techniques for modelling electrochemical energy storage (ES) devices in insular power network applications supported on real data. The first contribution is a comprehensive performance study between a set of competing electrochemical energy storage technologies: Lithium-ion (Li-ion), Nickel–Cadmium (NiCd), Nickel–Metal Hydride (NiMH) and Lead Acid (PbA) batteries. As a second contribution, several key engineering parameters with regards to the PbA battery-based storage solution are examined, such as cell charge distribution, cell string configuration and battery capacity fade. Moreover, an ES system operating criterion is discussed and proposed to manage the inherent rapid aging of the batteries due to their cycling activity, as a third contribution. The simulation results are supported on real data from two non-interconnected power grids, namely Crete (Greece) and São Miguel (Portugal) Islands, for demonstration and validation purposes.

Keywords: battery SOC; modelling techniques; insular grids; electrical energy storage; renewables integration.

---

1. Introduction

In the last decade and half CO_2 emission reduction has become an item on the political agenda of most developed countries to decelerate the global warming phenomenon. In this sense, renewable energy sources have a fundamental role towards climate change mitigation, the decrease of negative health and environmental effects and the security of electricity supply [1] [2].

Insular power grids (IPG) are encouraging for renewable energy sources (RES) deployment since wind and solar resources are generally abundant. Presently, RES exploitation in insular systems is an increasing reality, although it still has a reduced or moderate contribution to the insular energy mix. However, the gradual changes in insular energy mix will introduce new challenges from the grid operation perspective, mainly due to the intrinsic volatility of renewable generation exacerbated by load variability, inexistent interconnections and

* Corresponding author at Faculty of Engineering of the University of Porto, R. Dr. Roberto Frias, 4200-465 Porto, Portugal.
E-mail address: catalao@ubi.pt (J.P.S. Catalão).

reduced dimensions of the insular grids. In this framework, insular grid operators would need to resort to additional reserve margins in order to keep the reliability of the IPG intact [3]. For instance, if wind power integration surpasses 20% of the installed capacity, ancillary services such as frequency regulation would require an increase of 7% of capacity to face the grid instability [4]. For the aforementioned reasons additional sources of flexibility have to be adopted in order to avoid the deterioration of IPG management [5].

ES systems could become in the medium term one the main drivers for RES expansion in insular energy panorama. However, IPGs are indeed heterogeneous in terms of size, RES resources, load demand variability and installed power mix. ES can only become a viable solution if analysed in connection with the challenges associated to RES planning at a large scale [6] [7].

In this paper two real insular systems that serve as the basis for the present study are discussed. The next part targets a comprehensive study of four competing electrochemical storage devices, which are Li-ion, NiCd, NiMH and PbA batteries; their evaluation is performed on basis of merit figures created for this purpose. The third part is dedicated to the PbA battery. The design aspects of this battery sizing are analysed, specifically the charge distribution on a serial cells arrangement and energy capture as function of cells configuration (single or parallel strings). The paper ends with the presentation of an ES system operating criterion with the purpose of extending the battery life. The simulation results are supported on real data from non-interconnected power grids, which are Crete (Greece) and São Miguel (Portugal) Islands. The real data concerning one week of operation were supplied by the Singular EU FP7 project [8]. An ES system operating criterion is proposed and discussed to manage the inherent rapid aging of the batteries due to their cycling activity. A simplified modelling of the capacity fade estimation is also proposed and utilised in this paper.

The remainder of the paper is organised as follows. In section 2 the background on the studied conventional energy storage technology is addressed. In section 3 a summary of the two researched insular systems is presented and the respective case studies are addressed. Section 4 focuses on the analysis of the performance between a set of competing electrochemical ES technologies. The sensitivity analysis of battery design parameters is presented in Section 5. The conclusions are finally made in Section 6.

2. Background on the studied conventional energy storage technology

Utility ES applications will play three main roles [9] [10] [11] [12] : 1) Stabilizing power which means ES can make an active contribution to the grid power quality with sophisticated services aiming voltage and frequency regulation; 2) High flexibility in balancing power – for filling the gaps between conventional and non-conventional power, e.g., short-time drop in wind power can be replaced by ES resources. Alternatively, it can secure critical energy supply while part of generation is ramped-up or disconnected from the grid. Moreover, high flexibility means the energy discharge time can be chosen according to the application itself; 3) Dispatching energy which allows the possibility to deploy power when it is needed. Such solution offers opportunities to take advantage of time-pricing scheme since the energy can be stored at low demand periods and traded to be deployed at higher price periods, thus, shortening the payback time and increasing the potential profits.

Utility ES solutions comprise a range of technologies with wide-ranging energy and power handling capabilities [13]. Electrochemical batteries could offer the required flexibility to cope RES intermittency at all levels of the insular power grid [14] [15]. The support given by a battery energy storage system (BESS) is that it can recover the wind power curtailment and at same time providing advanced grid services concerning the discharge of electrical energy in a longer period or in a very short time [16]. On the other hand, the reduction of the utilisation of traditional power stations in favour of the use of RES raise questions of performance among the different electrochemical options and the optimal sizing of grid connected battery systems [17]. That said, one of main challenges for grid BESS successful operation is their ability for working for extended periods of time at a partial charge [18].

Currently, the battery universe for grid-scale ES systems as mature and commercially available solutions comprises PbA and Li-ion batteries. Despite their high media exposure and continuous improvement on the performance by many battery manufacturers other electrochemical ES options are available. That is the case for NiMH and NiCd batteries, however their application in the ES market varies greatly [19] [20]. Recently, Sodium Sulphur (NaS) batteries have been considered as model candidates for large grid scale BESS applications [21]. Although it is known that this battery is highly efficient and has environmentally friendly characteristics, it has several additional design requirements due to the operating conditions and cell configurations [22] which make the project and O&M costs of this BESS expensive for s small electric grid such as São Miguel. For this reason, NaS BESS are not considered in this study. However, a study of modelling and sizing of NaS BESS for extending wind power performance in Crete Island was performed in [23].

From a historical perspective PbA battery is the oldest technology in use. Its discover goes back to XIX century. The cycling characteristics and energy density of the PbA cell is inferior to other modern electrochemical options, but such issues are balanced in large part by the advanced level of maturity of the PbA battery industry and its low cost [24]. On the assumption that environmental issues and weight do not have an influence on the power generating facility, PbA batteries will likely remain a standard in the BESS field [25]. PbA batteries are utilised in a wide variety of different tasks, each with its own characteristic duty cycle ranging from combustion vehicles for starting the vehicle, as back-up in telecommunications and in other continuous power supplies. Such types of batteries are highly suitable for medium- and large-scale ES operations since they are capable to offer a satisfactory combination of performance parameters at a cost that is significantly below to those of other systems [26] for a large range of production capacity of electricity from RES [27]. In fact, several projects using this chemistry have been deployed in terms of medium- and large-scale grid ES systems, comprising installations of few hundreds of kW to MW. As an example, a 10 MW/40 MWh facility made up of PbA batteries has been running for more ten years [19]. Valve-regulated PbA (VRLA) batteries also known as advanced PbA batteries, which use an immobilised electrolyte, were developed to extend the service life and to minimise the maintenance when compared with conventional PbA batteries [18]. Advanced PbA display several advantages over conventional PbA batteries, such as higher reliability under depth of discharge (DOD) cycles, longer lifetime service and the flexibility of installation in any orientation [28]. Several projects are currently in motion concerning the application of such a BESS technology on islands, such as the Kahuku Wind Farm project - a 15 MW fully integrated ES and power management system designed to provide load firming for a 30 MW wind farm in Oahu, Hawaii, United States [29] or the Kaua‘i Island Utility Cooperative in Koloa Hawaii, United States [30].

Li-ion batteries present themselves as an alternative ES technology to PbA batteries and are becoming the main choice for many applications such as portable electronics, power tools, power back-up systems and plug-in hybrids and electric vehicles [31] [32] [33]. By the reason of having a long lifetime, higher specific or volumetric power, higher energy density, wide temperature range and decreasing costs have made Li-ion batteries more interesting for the abovementioned applications [34]. As for grid energy storage applications these electrochemical cells are getting increasing attention not only by the companies involved in their development but also the utilities seeking a reliable and lasting solution. The general interest around this chemistry is confirmed by several field trials across the globe. In USA, various pilot programs are conducting utility battery energy storage tests with Li-ion devices, the largest one located in a wind farm in California and featuring an energy storage installed capacity of 8MW/32MWh [35].

NiCd batteries have been used from early XX century. Such types of batteries display a significant power density and a lightly higher energy density when compared to other conventional ES technologies. Such types of batteries are able to perform well even in cases of low temperatures, i.e. from -20 °C to -40 °C. A Notable feature of chemistry NiCd is the capability to withstand high cycle durability. Such ability is associated to the chemical stability of the electrode materials. Typically, self-discharge is slow and remains relatively stable as result of progressive separator metallisation [36]. Nowadays, these batteries are gradually being dispelled due to the toxicity of cadmium, restricted to stationary ES usage in European space. However, recent developments indicate that this matter is being addressed, thus allowing this chemistry to be used in grid ES [37]. For instance, in Bonaire, a Caribbean Island, a NiCd battery based 3MW ES system is already in operation. The battery banks serve as storage interface between an 11MW wind power plant and a diesel/biodiesel fuelled thermal unit rated at 14MW, providing dependable and steady power supply [38].

NiMH is a technology that in the last decades was mostly neglected for grid storage purposes. The initial objective of NiMH batteries was to substitute the NiCd ones. Undeniably, the entire positive properties of NiCd batteries are displayed by NiMH batteries, except in the case of the maximal nominal capacity which is ten times lower than PbA and NiCd. The NiMH chemistry when compared to NiCd battery presents similar cycle durability and higher energy density yet much lower power rate capability. The power rate deterioration and capacity fade are caused by corrosion and fracturing of hydrogen-adsorbing alloy and cathode material changes into inactive crystalline form [36]. In turn, the self-discharge can be very low or moderate since the rate is strongly influenced by the utilised active materials [39]. Essentially, the reduced self-discharge capability of this chemistry is considered invaluable in some applications where energy conservation is crucial for electric systems operation. NiMH is considered robust and much safer when compared to Li-ion batteries. However, the prices between these two batteries are similar. Currently the progress investigation and development of NiMH battery materials has achieved noteworthy improvements in such domains as lifetime and operating temperature range that turns the NiMH battery into a feasible contender for utility-scale BESS utilisation [40].

3. Two Insular Systems as Case Studies

3.1 Crete, Greece

The Crete thermal generation is made of three thermal power plants (Atherinolakkos, Chania, Linoperamata) of circa 765 MW containing 25 generating units, all managed by the Public Power Corporation (PPC). Additionally, the non-conventional generation sources of about 194 MW are comprised by 32 Wind farms belonging to private entities. In conclusion, a large number of both rooftop and ground-mounted Photovoltaic (PV) systems have been commissioned in the last six years, which corresponds to a solar power of circa 95 MW. In annual terms, the energy needs of Crete is nearly 3 TWh and during summer the maximum power consumption ascends to 550-600 MW, as a result of the tourism factor. The transmission system is operated at 150kV and contains 19 power substations. In turn, at grid distribution level the electricity is supplied at 15kV and 20kV. RES based energy production exceeds just only 20% of the demand at least at certain times during the year, whereas in certain windy and/or sunny days the instantaneous RES energy injection reaches 50%.

In this island the customers of PPC are all the end users – PPC being the biggest electricity supply and power production company in Greece with circa 7.4 million customers in both the non-interconnected and interconnected power systems. The generation mix of Crete in the end of 2013 can be observed in Table 1.

"Table 1 can be observed at the end of the document".

In addition, the power system of Crete includes three additional thermal units that can enter into operation in case of emergency (e.g. generation shortfall) and presently serve as cold reserve units. The aforementioned thermal units comprise two CCGT units combining an installed capacity of 33.8MW and one steam turbine powered power plant rated at 6.2 MW.

In a medium-term perspective, energy production expansion comprises the installation of 2 new ICE units in the Atherinolakkos Power Station, consequently increasing the installed ICE capacity by 100 MW. Additionally, plans exist for installing a new 250 MW CCGT plant in Korakia area, (in the middle of the distance between Rethymno and Iraklio) in combination with a Natural Gas Terminal Station.

A. Scheduling strategies and reserves management

Scheduling strategies and reserves management on the subject of the unit commitment procedures, the thermal units can be split into 3 distinct classes: peaking units, mid-merit units and must-run units.

The initial category just includes OCGT units. The switch on/off decisions are made for a few hours ahead with just few minutes' refinements depending on the RES forecasting errors and load.

Mid-merit units contain the ICE units and their switch on/off decisions are effectuated for a few hours ahead with circa a quarter of an hour tweaks depending on the RES forecasting errors and load. Thus, cost functions are usually taken into consideration for such a decision.

The last category consists in the Steam units and the CCGT units and such type of units change their commitment status exclusively for maintenance purposes. Thus, the maintenance requirements are always communicated from the power stations operator to the dispatch centre operator. In order to select the best possible period of maintenance such requirements are taken into consideration along with demand estimations. The CCGT is the most flexible plant of this type of category explained by the fact that during the low load demand of the winter period one of the gas turbines (GT) of the CCGT block is switched off, thus, this GT could initiate its operation once more in cases of demand increases. Therefore, in case of Crete Island this is the main reason why one GT and the corresponding steam turbine (ST) of the CCGT plant are considered base-load units for the winter period.

The CCGT is typically utilised for frequency regulation in a context such as economic dispatch procedures. RES generation deviations and load demand are mostly addressed by this type of unit. Periodically, at every 5 to 15 min the operating point of the rest of the committed units might change in line with the fuel costs of the units – also compared with the CCGT additional cost.

Operators have real-time access to direction measurements and wind speed at each wind park. This not just regularly supports the assessment of the wind power production, but the probability of wind power generation fluctuations as well.

As for PV power plants, based on their geographical dispersion several properly selected PV plants are monitored and their production is then adapted to match the power generation resources of the island, with the intention of assessing the total PV generation.

The instructions of the dispatch are communicated to the operators of each conventional unit through dedicated carrier lines every time they are required. In case of regulating the reactive power production of the units resembling instructions are provided. Typically, the CCGT operates in load-following mode for frequency regulation.

Primary, secondary and tertiary spinning reserves are controlled by HEDNO. The spinning reserve requirements calculation takes mostly into consideration the possibility that at least the largest generating unit in operation trips since these are the minimum spinning reserve requirements. Spinning reserve requirements take also into consideration such parameters as a) the weather conditions, b) the wind power production, c) the wind direction (optionally), considering that for the same wind speed the wind production rises for south wind direction, and d) the possibility that a single transmission line is out of order.

B. RES management

Only in cases when the energy production comes from wind parks the process of curtailment is permitted. Since each PV plant has a small capacity and despite PVs being widespread, the fact that they produce during daytime period (when limited curtailment is expected) leads to such a policy for wind power. Ultimately, there is no preference on voltage levels.

Still on the subject of curtailment process – wind power plants have been separated into two groups: the old ones (Group A) that are not curtailed except if the new ones (Group B) minimise their output, set equal to zero. This signifies that except if all wind farms belonging in Group B have minimised their production, no wind park of group A will receive reduced set-points. The total set-point, the maximum total allowable wind production, is automatically calculated every 20 seconds based on the preferred wind power penetration level of the insular power system that is around 30-40% and the technical minimum of the committed conventional units. Therefore, the set-point of the online wind farms is calculated proportionally to their installed capacity. In this regard, the curtailment is mainly distributed to group B wind parks and any additional curtailment is distributed to group A wind parks.

3.2 São Miguel, Azores

It is the largest island of the Autonomous Region of the Azores (Portugal). EDA is the transmission/distribution system operator also in control for the thermal production in the island of São Miguel. The company that is in charge for renewable energy production is EDA Renováveis and comprises geothermal, small hydro and wind production. It possesses one thermal power plant containing eight ICE units with a total capacity of 98 MW and various RES plants (hydro, wind, PV, and geothermal) widespread across the island. In Table 2 is presented the generation mix of São Miguel at the end of 2014.

"Table 2 can be observed at the end of the document".

The Geothermal plants found on this island operate with constant power and do not support the frequency and voltage regulation. Similar operational patterns are shown by the seven small hydro plants, consequently not having much importance for the system management as a result of their small installed capacity.

The low-load periods which correspond to night periods are currently saturated with renewable energy: there is no margin for additional renewable production and, also, the wind production needs to be curtailed during such periods due to the need to keep the thermal units running over their technical minimum limits in order to guarantee the frequency and voltage regulation.

Forthcoming prospects include the building of a waste incineration plant (private investment) and perhaps additional geothermal capacity. Nonetheless, this will only be possible with the contribution of storage (reversible hydro units) in the system in order to reduce the over-generation during the low-load periods.

A. Scheduling strategies and reserves management

The load dispatch centre of the islands manages all the production facilities and notifies the thermal power plant (heavy-fuel oil) with approximately one hour earlier for the necessity to start/stop one of the smaller (4 x 7.7 MW) or one of the larger (4 x 16.8 MW) generation units. Yet, the operators of the thermal power plant are who decide which of the smaller units or which of the larger units could be started or stopped.

In addition, an original risk-based method was implemented and is presently constantly in operation, giving 24h ahead scheduling results for the dispatch centre operators of S. Miguel. The risk-based scheduling method delivers suggestions for the hourly commitment of generators (8 thermal generators), risk of load shedding, risk of wind shedding, and risk of operation below the technical minimum of the generating units. The risk-type information contains probability of occurrence and expected value of the occurrence and associated cost. At every hour, the dispatch centre operators ensure access to specific stochastic dispatch information, with complete information for each generator, about individual suggestions for dispatch generation and related risks and costs.

By knowing the characteristics of São Miguel's electric system and the characteristics of the available resources (two geothermal plants, seven small run-of-the-river hydro plants, one thermal heavy-fuel power plant and one wind farm), the dispatch of the generators follows a very simple process. The two geothermal plants function as base-load units, as they work at constant power and not being capable to change their output power and, consequently, such plants do not contribute to frequency and voltage regulation. Since the run-of-the-river hydro plants are small they are of negligible importance given the system size. Such systems operate at constant power depending on the available resource at each time interval. In this island storage dams do not yet exist.

The remaining power plants are the wind and the thermal power plant. It is essential to keep in mind that, very frequently, in low-load periods during night time the wind farm output is curtailed as a result of the saturation of the load diagram with renewable production which is mostly geothermal. The geothermal production cannot be limited or shutdown on a regular basis and due to the necessity to have several thermal generators operating and respecting their technical minimum in order to guarantee that enough spinning reserve is available.

The dispatch operators assess the expected system load and the system behaviour as far as one hour in advance and they offer instructions to the thermal power plant to start or stop the generators, regardless of the size.

No secondary reserve is deployed for the reserves identification. The system functions with a spinning reserve ratio always superior to 15-20%. Below this redline the dispatch operators instruct the thermal power plant to start-up supplementary generators. Also, a different characteristic that can influence the determination of the spinning reserve level is the real-time wind farm production. However, such action also highly depends on the sureness of the operators.

B. RES management

At present, since the power system on the island is particularly simple and the entire renewable and thermal production belongs directly or indirectly to the System Operator, the administration of the system, in what concerns this matter, is in fact quite simple. To begin with, there is not a presence of urgency for RES curtailment depending on the voltage level. The sole RES production typically curtailed is the one produced by the wind farm and it frequently takes place during low-load periods, as mentioned before. In such a case, the dispatch operators transmit a specific set-point to the wind farm with the purpose of restricting its maximum production, each time when it is required. The hydro and the geothermal power stations are prioritised regarding power production due to the characteristics of their output since it is exceptionally constant when compared to the wind farm power output that is much more uncertain and variable. Additionally, the technical features of the geothermal plants do not allow and/or do not recommend for changing its power output and/or starting/stopping recurrently.

4. Part 1: Performance Comparison of Electrochemical Batteries

4.1 Modelling Approach

Many methods can be utilised to model the operation of a battery and each method highlights precise operational characteristics: electrical, electrochemical and mechanical models. In the case of the electrochemical models – more importance is given to the electrochemistry of the active types and their contact with each other and with the interior membranes of the battery cells. As for the mechanical and electrical models – a black-box method is followed by them and thus it is analysed the interaction of the battery with the system of which is a part of.

Even though mechanical models have a higher importance when it comes to decide the installation and operational safety for batteries, the electrical models tend towards the assessment of the ability of incorporating the battery as an element in the electricity supply chain.

A. Electrochemical Model

The most important electrochemical model is inspired on Randles' equivalent scheme. It is made of a serial resistance R_s that symbolises the ohmic voltage drops in both electrolyte and electrode. The capacitance C_{DL} often called electric double layer capacitance represents the space charge which is manifested at the electrode–electrolyte interface.

Such type of charge is produced by the difference of internal potentials the electrolyte and electrode. Due to the low charge density in the electrolyte the correlation between both is nonlinear [41]. A different modelled parameter applies to the electrode voltage at thermodynamic equilibrium, labelled as the voltage source E_{th}. In conclusion, impedance designation Z_F defines the charge transfer effect at the electrode–electrolyte interface with the active material diffusion in electrolyte and electrode. In [42] it is possible to observe the equations of the electrochemistry which are seen as the foundation to the calculation of Randles' parameters.

B. Thevenin Model

Thevenin model is the most popular one since its depiction is considerably intuitive from the electrical point of view. A DC voltage source in series with a resistance is the representation of such battery model. On the other hand, leading to increased modelling complexity are the charge transfer occurrences associated with its own time constants. Due to the electric double layer phenomenon and in order to represent transient behaviour correctly, one or more resistor-capacitor circuit (RC) networks can be incorporated [43].

C. Advanced Thevenin Models

In order to elaborate a more accurate and advanced model of battery behaviour internal parameters have to be formulated considering the state of charge (SOC) dependency, parameters such as internal series resistance dependence on SOC or in the form of DOD and open circuit voltage (OCV) as a function of SOC [44]. Through the means of third-order polynomial curves for various discharge currents a different approach defines the battery voltage versus SOC [45]. By implementing the same method, the polynomial description includes two RC parallel networks for short and long time constants [46]. In such a model both electrochemical resistance and storage capacitance are approximated as continuous functions of OCV. The possibility of foreseeing both charging and discharging behaviour can be encountered in [47].

In cases such as the identification of parameters regarding Thevenin-based models, the techniques can be split into iterative numerical optimisation (e.g. [48], [49]) and online identification [50]. The iterative identification tools implement genetic and nonlinear least squares estimation algorithms which in turn require initial assumptions. The number of parameters to be assumed is generally high. The estimations required for starting the identification process made at the beginning are the main drawback of such methods. In other words, an incorrect guess could eventually become a local minimum. Additionally, the time spent on iterative simulations is also a disadvantage for a precise identification.

D. Zimmer Model

The Zimmer model was initially created in order to model the NiCd battery. However, more recently other electrochemical battery categories are under study using such type of model [51]. The equivalent circuit consist of two RC networks: one models the diffusion phenomenon and the other network defines the electrochemical ES. Additionally, every RC network parameters displays a dependence on SOC, temperature and current.

E. Harmonic Model

Created via signal excitation to obtain a harmonic response is the electrochemical accumulator model. Namely, by combining experimental impedance spectra with a numerical identification method a nonlinear equivalent circuit as function of load pulse frequency can be achieved. Such technique is researched in several studies for testing NiMH batteries [52], PbA batteries [50], [53], and Li-ion batteries [48]. Despite the fact, the same modelling method is possible to be utilised to set up the electrical behaviour regarding a proton exchange membrane fuel cell in which the diffusion impedance is modelled by two RC cells [49]. The harmonic model methodology creates fundamentally small signal models and this could be a limitation in large signal conditions due to the nonlinearities of the electrochemical batteries. Thus, as a result of the dependence of SOC on battery behaviour, it is highly demanding to have a result of an equivalent circuit at a mean current that is not zero.

4.2 NiCd battery

The electrochemical ES of this type is approximated by a Paatero model [53]. The terminal voltage consists of two parts. The open-circuit voltage U_{ocv} is given by:

$$U_{ocv}^{k} = a + b \times DOD_{Bat}^{k} + \left(c + d \times DOD_{Bat}^{k}\right) \times T^{k} \quad (1)$$

in which T^{k} represents the battery temperature at time instant *k*, DOD_{Bat}^{k} expresses the DOD at time instant *k* and where the *a*, *b*, *c* and *d* are constants to be found by laboratory tests. The second part of the terminal voltage expression is related with the calculation of overpotential voltage U_{op}^{k} as:

$$U_{op}^{k} = x_1 + x_2 T^{k} + x_3 DOD_{Bat}^{k} + x_4 \left|I_{Bat}^{k}\right| + \frac{x_5}{\left|I_{Bat}^{k}\right|} + \left(x_6 e^{x_7 DOD_{Bat}^{k}} + x_8\right) \times \left(e^{x_9 T^{k}} + x_{10}\right) \times \left|I_{Bat}^{k}\right| + x_{11} tan\left(x_{12} DOD_{Bat}^{k} + x_{12}\right) \quad (2)$$

in which the battery current at time instant is represented by I_{Bat}^{k} and the parameters to be determined in conjunction with the constants referred to Eq. 1 are represented by the x_i. In case of this study such constants are based on experimental data available in [53]. Then, merging Eq. 1 and Eq. 2, the battery terminal voltage U_{Bat}^{k} will be:

$$U_{Bat}^{k} = U_{ocv}^{k} - U_{op}^{k} \quad (3)$$

The battery capacity at time instant *k* is modelled as:

$$C_{Bat}^{k} = d_1 + e_1 \times I_{Bat}^{k} + f_1 \times arctan\left(g_1 + h_1 I_{Bat}^{k}\right) \quad (4)$$

in which d_1, e_1, f_1, g_1 and h_1 are defined as constants as stated in [53]. DOD_{Bat}^{k} is updated considering past DOD $\frac{1}{C} I_{Bat}^{k} \times \Delta t$ and present Coulomb-counting:

$$DOD_{Bat}^{k} = DOD_{Bat}^{k-1} + \frac{1}{C_{Bat}^{k}} I_{Bat}^{k} \times \Delta t \tag{5}$$

4.3 NiMH battery

Electrical circuit model for a single battery is presented in Figure 1, which is composed by two groups of capacitor and resistor networks and an internal resistance R_{Ω}. The $R_D C_D$ circuit is used to model the effects on the surface of the electrodes. The other pair, $R_K C_K$, takes into account the diffusion processes in the electrolyte [54]. Both RC networks are used to emulate the battery I-V transient response. The first RC network provides the short-time transient response while the second RC network mimics the long-term transient behaviour.

"Figure 1 can be observed at the end of the document".

Determination of R_{Ω}, R_D and R_K is performed applying a known load at a constant discharge current modulated as current pulse.

The voltage variation at battery terminals is used to measure the voltage components U_{Ω}, U_D and U_K associated to R_{Ω}, R_D and R_K. Finally, C_D and C_K electrical parameters are identified by measuring the time constants τ_D and τ_K with the modulate current.

As a result, U_{Bat}^{k} can be expressed as follows:

$$U_{Bat}^{k} = U_{\Omega} + U_{D}\left(1 - e^{-\left(\frac{k}{\tau_D}\right)}\right) + U_{K}\left(1 - e^{-\left(\frac{k}{\tau_k}\right)}\right) \tag{6}$$

Knowing the battery U_{ocv} a relation can be found to correlate with the NiMH battery SOC. Since the relationship between these two battery parameters is non-linear, a piecewise linearization strategy can be adopted as suggested in [55].

$$SOC_{Bat}^{k} = \begin{cases} a_1 U_{ocv}^{k} + b_1, & 0 \le U_{ocv}^{k} \le 0.1 \\ a_2 U_{ocv}^{k} + b_2, & 0.1 < U_{ocv}^{k} < 0.8 \\ a_3 U_{ocv}^{k} + b_3, & 0.8 < U_{ocv}^{k} \le 1 \end{cases} \tag{7}$$

Alternatively, SOC_{Bat}^{k} can be described involving measured electrical quantities and estimated internal constants. For discharging mode is defined as:

$$SOC_{Bat}^{k} = a_i U_{Bat}^{k} + a_i I_{Bat}^{k} \left(R_{\Omega} + R_D + R_K \right) + a_i I_{Bat}^{k} R_D e^{\frac{-k}{\tau_D}} + a_i I_{Bat}^{k} R_K e^{\frac{-k}{\tau_K}} + b_i \tag{8}$$

While for charging regime is evaluated by:

$$SOC_{Bat}^{k} = a_i U_{Bat}^{k} - a_i I_{Bat}^{k} \left(R_{\Omega} + R_D + R_K \right) - a_i I_{Bat}^{k} R_D e^{\frac{-t}{\tau_D}} - a_i I_{Bat} R_K e^{\frac{-t}{\tau_K}} + b_i \tag{9}$$

4.4 Li-ion battery

In case of the electric circuit modelling for Li-ion batteries, in [56] is presented the arrangement that can be observed in Figure 2 in which R_t is the internal resistance that includes all the resistances between electrodes while R_sC_s, R_fC_f and R_mC_m are the circuit time constants. R_t basically depends on I_{Bat}^{k} and consequently, it is assessed by the equation presented below:

$$R_t^k = 2.4572(I_{Bat}^{k}) - 0.6101(I_{Bat}^{k}) + 5.2497 \tag{10}$$

Parameters related to battery dynamic response are modelled by a quadratic relationship with SOC_{Bat}^{k}.

$$R_s^k = 72.42(SOC_{Bat}^{k})^2 - 104.15 SOC_{Bat}^{k} + 39.51,\ 0.525 < SOC_{Bat}^{k} \le 1 \tag{11}$$

$$R_s^k = 96.57(SOC_{Bat}^{k})^2 - 67.64 SOC_{Bat}^{k} + 13.69,\ \ 0 \le SOC_{Bat}^{k} \le 0.525 \tag{12}$$

$$R_m^k = 48.98(SOC_{Bat}^{k})^2 - 72.24 SOC_{Bat}^{k} + 30.12,\ \ 0.575 < SOC_{Bat}^{k} \le 1 \tag{13}$$

$$R_m^k = 23.28(SOC_{Bat}^{k})^2 - 16.18 SOC_{Bat}^{k} + 5.24,\ \ 0 \le SOC_{Bat}^{k} \le 0.575 \tag{14}$$

$$R_f^k = 11.76(SOC_{Bat}^{k})^2 - 17.59 SOC_{Bat}^{k} + 9.78,\ \ 0.575 < SOC_{Bat}^{k} \le 1 \tag{15}$$

$$R_f^k = 1.41(SOC_{Bat}^{k})^2 - 1.72 SOC_{Bat}^{k} + 2.11,\ \ 0 \le SOC_{Bat}^{k} \le 0.575 \tag{16}$$

"Figure 2 can be observed at the end of the document".

And short and long time constants calculations are expressed by:

$$\tau_s{}^{k} = \frac{1}{9.74(SOC_{Bat}^{k})^2 - 14.01 SOC_{Bat}^{k} + 6.09},\ \ 0.525 < SOC_{Bat}^{k} \le 1 \tag{17}$$

$$\tau_s{}^k = \frac{1}{8.03(SOC_{Bat}^k)^2 - 5.15SOC_{Bat}^k + 1.91},\ \ 0 \le SOC_{Bat}^k \le 52.5\% \tag{18}$$

$$\tau_m{}^k = \frac{1}{-20.94(SOC_{Bat}^k)^2 - 34.57SOC_{Bat}^k - 2.65},\ 0.575 < SOC_{Bat}^k \le 1 \tag{19}$$

$$\tau_m{}^k = \frac{1}{57.47(SOC_{Bat}^k)^2 - 56.42SOC_{Bat}^k + 23.74}, 0 \le SOC_{Bat}^k \le 57.5\% \tag{20}$$

$$\tau_f{}^k = \frac{1}{240.43(SOC_{Bat}^k)^2 - 371.62SOC_{Bat}^k - 220.03},\ 0.575 < SOC_{Bat}^k \le 1 \tag{21}$$

$$\tau_f{}^k = \frac{1}{451.9(SOC_{Bat}^k)^2 - 383.26SOC_{Bat}^k + 156.8}, 0 \le SOC_{Bat}^k \le 57.5\% \tag{22}$$

The fact that the SOC depends on U_{ocv} creates the necessity of experimental data with several battery current levels. This type of relation can be observed in [57]. It is evident that a variety of battery current conditions can be defined by a single curve fitting. Thus, the battery voltage is obtained from Eq. 23, 24 and 25.

$$U_{R_s \| C_s}^k = I_{Bat}^k R_s^k (1 - e^{\frac{-k}{\tau_s}}) + V_{sn0} e^{\frac{-k}{\tau_s}} \tag{23}$$

$$U_{R_m \| C_m}^k = I_{Bat}^k R_m^k \left(1 - e^{\frac{-k}{\tau_m}}\right) + V_{mn0} e^{\frac{-k}{\tau_m}} \tag{24}$$

$$U_{R_f \| C_f}^k = I_{Bat}^k R_f^k \left(1 - e^{\frac{-k}{\tau_f}}\right) + V_{fn0} e^{\frac{-k}{\tau_f}} \tag{25}$$

where V_{sn0}, V_{mn0} and V_{fn0} are the initial voltage at C_s, C_m and C_f respectively. Then, battery output U_{Bat}^k takes the form:

$$U_{Bat}^k = U_{oc}^k - I_{Bat}^k R_v^k - U_{R_s \| C_s}^k - U_{R_m \| C_m}^k - U_{R_f \| C_f}^k \tag{26}$$

4.5 PbA battery

By utilising one series resistance R and a single RC block for transient behaviour an electric network for modelling PbA type batteries can then be constructed. However, when operating at low charge/discharge, an additional RC block provides a better accuracy [58]. However, this representation does not consider the irreversible reactions that take place due to the electrolysis of water when the charging is ending.

A model description that takes into account this internal loss mechanism is proposed in [59] through the inclusion of a parasitic branch that soaks some of the input current when the battery has been charged. The equivalent electric network model is shown in Figure 3 where R_0 is the polarisation resistance, R_1C_1 is the short-term transient response, R_2C_2 is the long-term response, I_{Bat_m} is the current in the main branch and I_{Bat_p} is the parasitic branch current.

"Figure 3 can be observed at the end of the document".

In such type of model the elements of this circuit do not always depend on electrolyte temperature and battery SOC. On the other hand, it is assumed that time constants τ_1 and τ_2 remain unchanged.

U^k_{ocv} in equation 27 is defined as a electrolyte temperature θ^k and function of SOC.

$$U^k_{ocv} = U^0_{ocv} - K_E \left(273 + \theta^k\right)\left(1 - SOC^k_{Bat}\right) \tag{27}$$

The temperature has no influence on the internal parasite resistances which are only affected by SOC.

$$R^k_0 = R_{00}[1 + A_o(1 - SOC^k_{Bat})] \tag{28}$$

$$R^k_1 = -R_{10}\ln(SOC^k_{Bat}) \tag{29}$$

$$R^k_2 = R_{20}\frac{\exp[A_{21}(1 - SOC^k_{Bat})]}{1 + \exp(\frac{A_{22}I^k_{Bat_m}}{I^N_{Bat}})} \tag{30}$$

in which I^N_{Bat} is the nominal battery current, $I^k_{Bat_m}$ is the current flowing in the main branch and U^0_{ocv}, K_E, R_{00}, A_0, R_{10}, R_{20}, A_{21}, A_{22}, are constants acquired from battery experimental tests. Dependence of the $I^k_{Bat_p}$ on the $U^k_{Bat_p}$ is governed by a strong non-linearity. On way is to approximate through the Tafel gassing current equation [60]:

$$I^k_{Bat_p} = U^k_{Bat_p} G_{po} \exp\left(\frac{U^k_{Bat_p}}{V_{po} + A_p\left(\frac{1 - \theta^k}{\theta_f}\right)}\right) \tag{31}$$

in which G_{po}, V_{po}, A_p are constants assessed by experimental procedures, $U_{Bat_p}^{k}$ is the voltage at parasitic branch, θ_f represents the electrolyte freezing temperature and θ^k is the electrolyte temperature at time k.

4.6 Case Study

In this section the set of electrochemical ES under study are subject to a comparative assessment through a frame of metrics of evaluation. Such merit figures provide an insight on the charging and discharging capability of the batteries according to different arranges. In one case, the ES structures performance considering a variable number of battery cells is investigated. In other case, it is explored the performance impact as function of the number of parallel strings. In addition, an analysis is performed concerning the impact of the sizing of the storage structures with a fixed number of cells.

The models are combined in cell banks and imitate an ES that has to respond to the demands of the grid. Thus, the operation strategy works by charging the battery with the excess generated energy at times of low demand with the purpose of being released at times of high demand. In this sense the batteries charge solely to eliminate renewable curtailment. The basic battery features for modelling parameters are shown in Table 3 [57] [61].

"Table 3 can be observed at the end of the document".

A. Metrics of evaluation

The electrochemical storage technologies under analysis are characterised by two performance merit figures. One deals with their ability to storage the wind power in excess when available and the other with the response capacity to demand needs. In this sense, it is proposed the storage efficiency index (*SEI*) and demand response index (*DRI*) which respectively calculate the percentage of charging and discharging excess power of the battery.

$$SEI = \frac{\sum E_{Bat_{IN}}^{k}}{\sum E_{WP_{Gen}}^{k} - \sum E_{WP_{Grid}}^{k}} \tag{32}$$

$$DRI = \frac{\sum E_{out}^{k}}{\sum E_{Dem}^{k} - \sum E_{WP_{Grid}}^{k}} \tag{33}$$

where $\sum E_{Bat_{IN}}^{k}$ is the energy counting referring to the battery input, $\sum E_{out}^{k}$ is the energy counting referring to the battery output, $\sum E_{WP_{Gen}}^{k}$ is the gross wind power generation, $\sum E_{Dem}^{k}$ is the energy consumption referring to the final consumers and $\sum E_{WP_{Grid}}^{k}$ is the wind power consumed by the grid.

B. Single string with fixed number of cells

To evaluate the capability of different battery types for large-scale ES each model is executed by means of the same initial parameters but adjusting the battery type variable in each case. The SOC for each type is initially set at 20% and in this test each BESS is designed with 500 identical cells. The outcomes are provided in Table 4 and Table 5 which show the final SOC at the end of the time horizon.

The acquired capability indicators show how the low charge and discharge rates of the PbA battery significantly decrease its performance, signifying that it will not efficiently utilise the generated power to meet the demand. The battery with the lowest cyclic performance reduction and therefore the longest life is the NiCd, which has the highest SEI and DRI numbers. NiCd also generates a high final SOC, signifying that the battery is 'self-sufficient' within the time period so is less likely to necessitate an occasional 'booster' charge from an external source. Measuring the final SOC is not, however, a realistic method for assessing the battery performance as it will be offset by the periods of time at which the battery is at minimum or maximum capacity.

"Table 4 can be observed at the end of the document".

"Table 5 can be observed at the end of the document".

C. Single string with variable number of cells

The comparison of performances of the studied batteries regarding São Miguel Island is shown in both Figures 4 and 5. As can be observed in the aforementioned scenarios the SEI indicator increases with the number of cells until a limit is reached. As for DRI performance, the NiCd battery is the single battery type which can conserve 100% DRI, even though Li-ion and NiMH are considerably close. The corresponding simulations associated to Crete are shown in Figure 6 and Figure 7.

"Figure 4 can be observed at the end of the document".

"Figure 5 can be observed at the end of the document".

"Figure 6 can be observed at the end of the document".

"Figure 7 can be observed at the end of the document".

According to the results of this study, the PbA battery seems to be the least appropriate for both power grids. To maintain demand capability with any battery except PbA the number of cells could be as low as five. To make an effective utilisation of the storage capacity and keep as much generated energy as possible an appropriate number of cells would be three strings of 10 (São Miguel).

In case of larger systems, the required number of cells may need to be increased. In the case of Crete, since requires a much larger size, approximately 2000 cells would be needed.

Regardless of performing better, NiCd batteries need to be handled with caution since they are built with heavy metals: cadmium and nickel. Both pose a threat to human health and the environment. Such batteries also suffer from what is called lazy battery effect which prevents them to receive more charge [61]. However, this is not a technical limitation anymore if adequate maintenance procedures are used as part of the ES management system.

D. Configuration in parallel strings

In this subsection both indicators are evaluated from an angle of arrangement of cells in strings (each string is made by 120 cells of the battery in series). The Li-ion battery model is used as a comparison for both islands.

Figure 8 and 9 show the DRI and SEI performance in function of number of strings. In the case of São Miguel system, DRI maximum is achieved for range of strings up to 10. Above this number the power storage is oversized which is reflected in the degradation of the indicator performance due to the reason of the cells being partially utilised. Thus, the curtailment power from RES that can be stored in this number of cells is manifestly low in face of the additional storage power. Therefore, the response capacity (DRI) of the battery compound diminishes concerning the expected storage capacity. Naturally, Crete has a significantly bigger island and by having a more complex electricity grid and also has a higher penetration of RES intermittent energy. Therefore, the DRI response remains high by surpassing 90% for the large majority of the studied combination number of strings. Certainly, if the window of the studied number of strings is increased the DRI decline will follow a similar tendency as São Miguel.

The SEI versus the number of strings can be seen in Figure 9. It is observable for the BESS performance in the case of São Miguel the capture rate for the storage is superior until a certain limit since the majority of the curtailed wind power is effectuated during the night-time period where a reduced consumption is verified. On the other hand, in Crete the scenario is more complex due to the reason that depending on the time of the year and the period of the day harnessing the excess of energy is highly restricted as mentioned in [23]. For instance, in January, the wind generation happens to be more active during the night and consequently exceeding, by a factor of two, several times the level of wind curtailment in comparison with the rest of period of the day. This highlights the fact that during the winter season the installed wind capacity is excessive during periods of low loads. On the other hand, during summer months such as August, the wind curtailment profile displays an inverse tendency since the curtailment peaks are higher during the day than during the night. This explains why the SEI has a lower rate in the case of Crete when compared with São Miguel.

"Figure 8 can be observed at the end of the document".

"Figure 9 can be observed at the end of the document".

5. Part 2: Sensitivity Analysis of Battery Design Parameters

5.1 Description of the PbA battery

Obtained through experimental tests in [62], the modelling approach chosen provides a direct way to relate SOC and battery current to battery service temperature.

A. Usable chemical capacity

A requirement for electrochemical ES device is its ability to satisfy power/energy constraints of a specific application. The energy available in a battery, designated as the battery capacity is quantified in ampere-hours (Ah) or in watt-hours (Wh) which is calculated by integral of battery voltage multiplied by current over the discharge period. On the other hand, usable capacity can be defined as the capacity available under the known load conditions until voltage reaches the minimum acceptable voltage without causing permanent damage to the battery.

Additionally, the actual temperature environment of a device has a significant influence on battery's internal impedance, which in turn has an impact on usable capacity. Usable capacity estimation is adopted in the present study as in the following equation [62] [63]:

$$C_{Bat}^{k} = \frac{C_{Bat}^{N}}{1 + 0.67\left(\frac{\left|I_{Bat}^{k}\right|}{I_{10}}\right)^{0.9}} \tag{34}$$

where I_{10} is the current used to discharge the battery in 10 hours, nominal capacity is expressed by C_{Bat}^{N} ,C_{Bat}^{k} is the ampere-hours capacity at instant k and I_{10} is the discharge current referred to a time period of 10h at 25ºC. In turn, C_{Bat}^{N} is given by:

$$C_{Bat}^{N} = 1.67 C_{10}\left(1 + 0.005\Delta T\right) \tag{35}$$

where ΔT is the present temperature subtracted from the temperature reference at 25ºC and C_{10} is the battery capacity when it is discharged in 10 hours.

B. Chemical capacity degradation modelling

Power rate and capacity characteristics of an electrochemical energy storing device tend to fade as the battery ages. Many aspects of how it is operated determine the evolution of the energy storing capacity deterioration. Not only how often the electrochemical storing device is cycled contributes to its aging, but also the charge and discharge rates, its charge level, operation in a wide range of temperatures and environmental conditions [64] [65]. Furthermore, the load cycle properties have also a critical role on this process. That is to say, if it is allowable for the battery to be operated at extremes states, i.e., over-charged or under-charged, or if the nature of load requires high-current pulses or steady discharging [66].

The capacity fade phenomenon happens when the electrode active materials start to lose their properties along with growing corrosion of their elements. In the corrosion process the lead based electrode will be gradually converted into lead dioxide (PbO_2) and lead (II) oxide (PbO). A visible consequence of undergoing oxidation is the rise of the internal impedance of the cells [67].

Due to the great effort to gather such data, developing a full model to predict battery failure is a complex matter. While the others aforementioned factors have an important role in the cell aging mechanisms, the active material losses are inherently related with consecutives discharging and charging operations of the PbA battery. Therefore, power cycling has a major impact on the loss of chemical capacity and impedance increase [68]. Hence, lifetime estimation in this paper adopts the traditional approach based on cycle counting at specific DOD that would lead to a certain capacity fade. In this context, there are several published studies. For instance, batteries testing based data plots can be consulted in [69] revealing the energy pattern cycled at different power levels for a wide range of DODs. This kind of plot is commonly built as indicative lifetime tool. It can be generally approached by the equation given bellow [70]:

$$F_{cy} = a_1 + a_2 e^{-a_3 DOD} + a_4 e^{-a_5 DOD} \tag{36}$$

where F_{cy} are the cycles for a specific DOD that lead the battery to failure and a_i are the model parameters which can be found in [70].

Usually, the conventional practice by the battery manufactures to declare the battery end-of-life consists in establishing a figure for the capacity permanent reduction of its rated capacity. Some manufacturers propose as reference number a reduction of 40%. Others suggest using a lower capacity reduction to 20%. In this sense, several studies demonstrate that for this interval the capacity loss of the battery decreases almost linearly [71] [72] [73]. In the present study, the end-of-life is set to 40% reduction. It is intended to establish a linear between the value of the capacity fade and the number of cycles of the battery activity for this operational range. The calculation of the capacity degradation is performed by the following expression:

$$C_{loss} = C_{Bat}^{N}\left[1-\left(\frac{0.4}{F_{40\%}}\right)\cdot N_{cy}\right] \tag{37}$$

where C_{Bat}^{N} designates the nominal capacity, $F_{40\%}$ are the cycles correspondent to a reduction of 40% in the battery capacity and N_{cy} refers to the cycle counting.

C. Coulomb efficiency

It is a merit figure that performs a ratio between the numbers of charges delivered to battery in charging mode with regards to the number of charges released in discharging mode.

Coulombic efficiency's reduction main cause has to do with the separation of water into oxygen called water electrolysis, making the electrons movement more and more difficult in an electrochemical system. Normally this efficiency surpasses the 95%. According to [74] the discharging efficiency can be modelled with losses as shown in the following equation:

$$\eta_d = 1 \tag{38}$$

By considering the opposite state, that is to say when it is being charged, the effective charges that are converted into stored electrochemical energy is conditioned by the battery SOC and charge current. If SOC is low, it means that the charging efficiency is almost complete. On the contrary, proceeding to charge at a very high SOC the process efficiency deteriorates significantly. Such pattern is described as follows [74]:

$$\eta_{ch}^{k} = 1 - exp\left[\left(\frac{20.73}{\frac{I_{Bat}^{k}}{I_{10}}+0.55}\right)\left(SOC_{Bat}^{k}-1\right)\right] \tag{39}$$

In Figure 10 the charging efficiency curve can be observed as a function of the battery current.

"Figure 10 can be observed at the end of the document".

D. SOC

The battery charge level monitoring complies with the SOC formulation presented below:

$$SOC_{Bat}^{k}=\begin{cases}\dfrac{Q}{C_{Bat}^{k}}\eta_{ch}^{k}, & I_{Bat}^{k}>0\\ 1-\dfrac{Q}{C_{Bat}^{k}}\eta_{dis}^{k}, & I_{Bat}^{k}<0\end{cases} \tag{40}$$

where Q represents the charge in movement while C_{Bat}^{k} is the usable capacity at time instant k. The last three equations can be merged into a single equation as follows:

$$SOC_{Bat}^{k}=\begin{cases}SOC_{Bat}^{k-1}+\dfrac{Q}{C_{Bat}^{k}}\eta_{ch}^{k}, & I>0\\ SOC_{Bat}^{k-1}+\dfrac{Q}{C_{Bat}^{k}}, & I<0\end{cases} \tag{41}$$

The grid battery system SOC is subject to the constraint:

$$0.2 \le SOC_{Bat}^{k} \le 0.9 \tag{42}$$

E. Battery terminal voltage

Current-voltage response follows a battery model proposed in [49]. The supplying charge battery terminal voltage is given by:

$$U_{Bat\_dis}^{k}=n_{cell}\cdot\left[1.965+0.12\cdot SOC_{Bat}^{k}\right]-n_{cell}\frac{|I_{Bat}^{k}|}{C_{10}}\cdot\left(\frac{4}{1+|I_{Bat}^{k}|^{1.3}}+\frac{0.27}{(SOC_{Bat}^{k})^{1.5}}+0.02\right)\cdot(1-0.007\cdot\Delta T) \tag{43}$$

The switching to charging mode voltage output is represented by:

$$U_{Bat\_ch}^{k}=n_{cell}\cdot\left[2+0.16\cdot SOC_{Bat}^{k}\right]+n_{cell}\frac{I_{Bat}^{k}}{C_{10}}\cdot\left(\frac{6}{1+(I_{Bat}^{k})^{0.86}}+\frac{0.48}{\left(1-(SOC_{Bat}^{k})\right)^{1.2}}+0.036\right)\cdot(1-0.025\cdot\Delta T) \tag{44}$$

where the number of battery cells is given by n_{cell} .

5.2 Case study

In this section are presented the results of the simulations carried out with the PbA BESS model. The findings cover charge distribution over a sample of cells arranged in series, single string versus multiple string arrangement and battery capacity loss. Finally, a BESS operating criterion is evaluated in order to increase the battery life time through lower battery cycling activity.

The virtual battery plant is made of 20 batteries, each one being designed with 48 cells. For the battery the rated capacity is 96Ah. All the storage capacity reaches 1920Ah. The battery management method consists in storing the wind power not absorbed by the grid at low-peak hours when the demand is reduced. In the hours when the consumption is higher the energy is released. The load demand and power generation data were sampled every 15 minutes. This means the readings are assumed as constant until the next sampling time. The PbA battery modelling parameters are depicted in Table 6 [57] [61].

"Table 6 can be observed at the end of the document".

5.2.1 Electrochemical cell organisation in strings

Due to the intermittence of wind power in terms of duration and magnitude, full charging of the batteries may not be possible if the size is not carefully selected. For instance, in short time periods, it is likely that parts of the cells are more stressed in terms of charging cycles in comparison to other cells of the same battery. Consequently, due to a higher cycling activity some of the cells will age early jeopardizing the battery performance with a premature reduction of storage capacity. Having that said, cell organisation impact is assessed in this context by thoroughly examining mono-string versus multiple-string structures. Furthermore, the simulations are performed with initial SOC mismatches among the cells of the same structure.

A. Mono string

In this configuration a structure of 48 PbA cells are serialized and subject to successive charge cycles. The SOC of every cell is tracked and the cycling activity is registered. Figure 11 shows the evolution of SOC for every cell. The flux line based representation highlights what happens for the cells in the chain. For the ideal case, in which energy capacity is identical for all cells, charging process is done sequentially cell by cell.

"Figure 11 can be observed at the end of the document".

As it can be seen, the nearest cells to the positive electrode are charged, in average, above 98% of their nominal capacity. On the other hand, the cells at the end of the string are penalised by their location, receiving much less charge. In fact, some of them are not being charged at all.

Equally, in Figure 12 the cycling activity can be seen. When charging the frailest cells, regarding capacity, these are the first to fill up since there is less to fill. Similarly, as the battery changes its operation to release charge, the first cells to become empty are those whose capacity is lower among the electrochemical set. In sum, the cells characterised by a lower capacity will drain faster and thus, accelerating their capacity loss rate, given that the cycling activity is more intense in relation to the higher capacity of the strongest cells.

"Figure 12 can be observed at the end of the document".

B. Parallel strings

Three strings comprising 16 cells each one make up the test assembly. Figure 13 and Figure 14 depict cells SOC and respective cycling activity. As expected the charge distribution observed in a cell string produces a similar result discussed in previous item. Because of its parallel configuration the strings receive an identical charge profile.

The organisation of the cells in parallel strings offers a higher charge rate. In other words, for the same number of electrochemical cells more wind power surplus energy can be processed and converted into stored chemical energy. As for cycling activity, Figure 14 supports the point of view of a more efficient allocation of charge distribution.

"Figure 13 can be observed at the end of the document".

"Figure 14 can be observed at the end of the document".

In sum, the cell configuration in terms of connection has a significant impact on charge distribution by increasing the use of certain cells to the detriment of others. Then, it is expected a decrease in BESS usable capacity due to a non-uniform cycling activity. In addition, cells parallel arrangement offers a higher performance.

5.2.2 Renewable energy surplus level based charging criterion

Maintaining high cycling activity, independently of the battery SOC, to support as much as possible the grid with ES from surplus wind power will accelerate the electrochemical ES degradation due to the chemical capacity loss. Moreover, even if the battery systems are operated at a high partial SOC the capacity degradation is unavoidable. Therefore, it is crucial to concentrate efforts on an operating strategy that meets the goal of recovering as much as possible the wind power curtailment, and at the same time, able to restrict the charging activity of the battery. To meet this challenge, one way is to define a wind power surplus level based charging criterion instead of performing charging continuous actions whenever the condition $P_{Gen}^{k} > P_{Load}^{k}$ is met and the batteries are not full charged. The charging criterion is implemented using as reference the renewable power curtailment over the demand. Consequently, different levels of ratio can be evaluated by counting the cycles of charge.

Figures 15 and 16 show the number of cycles executed when ratio based criterion is incremented up to 10%. In the first figure is accounted the average cycle number. As for the second, it reveals the record concerning the maximum number of cycles.

"Figure 15 can be observed at the end of the document".

"Figure 16 can be observed at the end of the document".

As can be seen, the criterion application led to a different cycling operation profiles for the two insular systems. In both systems, an improvement on the battery life can be achieved. On São Miguel Island the impact is dramatic, providing an economy higher than 80% if the criterion is chosen above the 4%. However, for the Crete Island the performance result is, in fact, far more modest around 10% considering the same range of percentage based criterion.

On the other hand, assigning a specific value for the criterion needs to take into account the maximisation of the installed capacity which means a high SOC is desirable. Considering the same range of values for the criterion, average SOC regarding the Crete insular system was examined and the outcome is presented in Figure 17. As a starting point, the BESS is charged initially at 35%. From the plot, it is clear a steep drop in SOC if the criterion goes above the 6%. By choosing the highest segment of the curve we get a battery system almost under exploited with 90% of the capacity to be wasted, but if the criterion based operating strategy is ignored the high number of cycling is expected to lead the storage facility to premature aging concerning its capacity loss. An optimal solution that satisfies a compromise between a high partial SOC and extends the ES operationally can be found by crossing the information provided by the Figures 15 and 17. In fact, as an adequate charging criterion a ratio number about 4% allows the SOC to be close to 80%. In this respect, it is considered the adequate choice.

"Figure 17 can be observed at the end of the document".

6. Conclusion

This paper has addressed the performance of electrochemical batteries to support grid with surplus wind power in insular systems. São Miguel (Azores) and Crete (Greece) served as the study basis. Two complementary investigations were thoroughly presented and discussed. The first part of the study focused on four electrochemical ES technologies (Li-ion, NiCd, NiMH and PbA). The reason these four different chemistries were chosen was to compare one of the most preferred solutions by the industry and academia (Li-ion) with the most historically employed one for general applications (PbA) and with two relatively recent and not so common chemistries (NiCd and NiMH). These last two had some drawbacks due to environmental reasons (especially in the case of NiCd) and requirements of complex charging protocols, but have been gaining a renewed interest since the new improved products commercialised by some enterprises have redirected the improvements also to grid-scale energy storage uses. The foundation tools for this analysis were the electric models provided by the literature. The comparison was made through two metrics that were developed in order to evaluate and provide an insight on the charging and discharging capability of the analysed technologies according to different arranges - the SEI and DRI. The ES structures performance considering a variable number of battery cells was investigated and the performance impact was explored as a function of the number of parallel strings.

In addition, an analysis was performed concerning the impact of the sizing of the storage structures with a fixed number of cells or as an alternative – a single string with variable number of cells. From the simulation results the NiCd battery has shown a higher performance when compared to other chemistries under study. This conclusion was supported on the basis of the metrics developed for this purpose. The Li-ion battery technology has shown a slightly inferior performance due to its lower ability to respond to load demand for identical storage size. Although the NiCd performed better, there are several issues to solve which are the presence of the heavy metal cadmium element, toxic for health reasons, and the memory effect that requires an elaborated ES management system. Both indicators are now used to compare the performance of Li-ion battery according to the number of strings. In the case of Crete the DRI response remains high by surpassing 90% for the large majority of the studied combination number of strings, while for São Miguel it is only maintained high for a low number of strings and then drops. However, the SEI has shown a lower rate in the case of Crete when compared with São Miguel since Crete is a bigger island. This happens due to the reason that harnessing the excess of energy is highly complex since it depends on the time of the year and the period of the day.

In the second complementary research line, some design parameters (SOC and number of charging cycles for mono and parallel strings) of the PbA battery were observed in order to assess their impact on ES applications. The cell configuration in terms of connection showed a significant impact on the charge distribution by increasing the use of certain cells in the detriment of others. Therefore, it is expected a decrease in BESS usable capacity due to a non-uniform cycling activity, which will provoke an accelerated ageing of a part of battery cells in disadvantage of others. In addition, cells parallel arrangement offers a higher performance. Since the batteries' life time is one of most sensible project variables for justifying their deployment, a criterion to regulate the ES bank cycling operation was proposed. The criterion works by triggering the battery energy transit on the basis of certain excess of renewable energy. Thus, an excess factor of circa 4% can lower the number of operation cycles by 10% for Crete and by 80% for São Miguel.

Acknowledgements

This work was supported by FEDER funds through COMPETE 2020 and by Portuguese funds through FCT, under Projects FCOMP-01-0124-FEDER-020282 (Ref. PTDC/EEA-EEL/118519/2010), POCI-01-0145-FEDER-016434, POCI-01-0145-FEDER-006961, UID/EEA/50014/2013, UID/CEC/50021/2013, and UID/EMS/00151/2013. Also, the research leading to these results has received funding from the EU Seventh Framework Programme FP7/2007-2013 under grant agreement no. 309048.

Bibliography

[1] M. Ranaboldo, B. D. Lega, D. V. Ferrenbach, L. Ferrer-Martí, R. P. Moreno and A. García-Villoria, "Renewable energy projects to electrify rural communities in Cape Verde," *Applied Energy,* vol. 118, pp. 280-291, 2014.

[2] A. S. Brouwer, M. v. d. Broek, W. Zappa, W. C. Turkenburg and A. Faaij, "Least-cost options for integrating intermittent renewables in low-carbon power systems," *Applied Energy,* vol. 161, pp. 48-74, 2016.

[3] A. Schroeder, "Modeling storage and demand management in power distribution grids," *Applied Energy,* vol. 88, no. 12, pp. 4700-4712, 2011.

[4] D. Milborrow, "Impacts of wind on electricity systems with particular reference to Alberta," in *Southern Alberta Alternative Energy Partnership Tech. Rep.*, 2004.

[5] E. Rodrigues, G. Osório, R. Godina, A. Bizuayehu, J. Lujano-Rojas and J. Catalão, "Grid code reinforcements for deeper renewable generation in insular energy systems," *Renewable and Sustainable Energy Reviews,* vol. 53, pp. 163-177, 2016.

[6] M. Kapsali, J. Kaldellis and J. Anagnostopoulos, "Investigating the techno-economic perspectives of high wind energy production in remote vs interconnected island networks," *Applied Energy,* vol. 173, pp. 238-254, 2016.

[7] H. Meschede, P. Holzapfel, F. Kadelbach and J. Hesselbach, "Classification of global island regarding the opportunity of using RES," *Applied Energy,* vol. 175, pp. 251-258, 2016.

[8] SiNGULAR, "Smart and Sustainable Insular Electricity Grids Under Large-Scale Renewable Integration," Grant Agreement No: 309048, FP7-EU, 2015. [Online]. Available: http://www.singular-fp7.eu/home/. [Accessed 2015].

[9] Y. Makarov, P. Du, M. Kintner-Meyer, C. Jin and H. Illian, "Sizing Energy Storage to Accommodate High Penetration of Variable Energy Resources," *IEEE Transactions on Sustainable Energy,* vol. 3, no. 1, pp. 34-40, 2012.

[10] S. Vazquez, S. Lukic, E. Galvan, L. Franquelo and J. Carrasco, "Energy Storage Systems for Transport and Grid Applications," *IEEE Transactions on Industrial Electronics,* vol. 57, no. 12, pp. 3881-3895, 2010.

[11] V. Boicea, "Energy Storage Technologies: The Past and the Present," *Proceedings of the IEEE,* vol. 102, no. 11, pp. 1777-1794, 2014.

[12] A. Schäfer, H. Schuster, U. Kasper and A. Moser, "Chapter 3 - Challenges of Power Systems," in *Electrochemical Energy Storage for Renewable Sources and Grid Balancing*, P. T. Moseley and J. Garche, Eds., Elsevier, Amsterdam, 2015, pp. 23-32.

[13] E. M. G. Rodrigues, C. A. S. Fernandes, R. Godina, A. W. Bizuayehu and J. P. S. Catalão, "NaS battery storage system modeling and sizing for extending wind farms performance in Crete," in *2014 Australasian Universities Power Engineering Conference (AUPEC)*, Perth, WA, 2014.

[14] E. Rodrigues, R. Godina, S. Santos, A. Bizuayehu, J. Contreras and J. Catalão, "Energy storage systems supporting increased penetration of renewables in islanded systems," *Energy,* vol. 75, pp. 265-280, 2014.

[15] A. Price, "Chapter 1 - The Exploitation of Renewable Sources of Energy for Power Generation," in *Electrochemical Energy Storage for Renewable Sources and Grid Balancing*, P. T. Moseley and J. Garche, Eds., Amsterdam, Elsevier, 2015, pp. 3-12.

[16] F. Luo, K. Meng, Z. Y. Dong, Y. Zheng, Y. Chen and K. P. Wong, "Coordinated Operational Planning for Wind Farm With Battery Energy Storage System," *IEEE Transactions on Sustainable Energy,* vol. 6, no. 1, pp. 253-262, 2015.

[17] E. M. G. Rodrigues, R. Godina, T. D. P. Mendes, J. C. O. Matias and J. P. S. Catalão, "Influence of Large Renewable Energy Integration on Insular Grid Code Compliance," in *Technological Innovation for Cloud-Based Engineering Systems*, Caparica, Portugal, Springer International Publishing, 2015, pp. 296-308.

[18] B. McKeon, J. Furukawa and S. Fenstermacher, "Advanced Lead–Acid Batteries and the Development of Grid-Scale Energy Storage Systems," *Proceedings of the IEEE,* vol. 102, no. 6, pp. 951-963, 2014.

[19] D. Enos, "Chapter 3 - Lead-acid batteries for medium- and large-scale energy storage," in *Advances in Batteries for Medium and Large-Scale Energy Storage*, United Kingdom, Woodhead Publishing, 2015, p. 57–71.

[20] Z. Huang and G. Du, “Chapter 4 - Nickel-based Batteries for Medium-and Large-Scale Energy Storage,” in *Advances in Batteries for Medium and Large-Scale Energy Storage*, United Kingdom, Woodhead Publishing, 2015, pp. 73-90.

[21] K. Jung, S. Lee, G. Kim and C.-S. Kim, “Stress analyses for the glass joints of contemporary sodium sulfur batteries,” *Journal of Power Sources,* vol. 269, pp. 773-782, 2014.

[22] J. K. Min, M. Stackpool, C. H. Shin and C.-H. Lee, “Cell safety analysis of a molten sodium–sulfur battery under failure mode from a fracture in the solid electrolyte,” *Journal of Power Sources,* vol. 293, pp. 835-845, 2015.

[23] E. Rodrigues, G. Osório, R. Godina, A. Bizuayehu, J. Lujano-Rojas, J. Matias and J. Catalão, “Modelling and sizing of NaS (sodium sulfur) battery energy storage system for extending wind power performance in Crete Island,” *Energy,* vol. 90, no. 2, pp. 1606-1617, 2015.

[24] S. Matteson and E. Williams, “Residual learning rates in lead-acid batteries: Effects on emerging technologies,” *Energy Policy,* vol. 85, pp. 71-79, 2015.

[25] M. Greenleaf, O. Dalchand, H. Li and J. P. Zheng, “A Temperature-Dependent Study of Sealed Lead-Acid Batteries Using Physical Equivalent Circuit Modeling With Impedance Spectra Derived High Current/Power Correction,” *IEEE Transactions on Sustainable Energy,* vol. 6, no. 2, pp. 380-387, 2015.

[26] D. A. Rand and P. T. Moseley, “Chapter 13 - Energy Storage with Lead–Acid Batteries,” in *Electrochemical Energy Storage for Renewable Sources and Grid Balancing*, Elsevier, Amsterdam, 2015, pp. 201-222.

[27] R. Megateli, G. Idir and A. Arab, “Study of the variation of the specific gravity of the electrolyte during charge/discharge cycling of a lead acid battery,” in *2015 3rd International Conference on Control, Engineering & Information Technology (CEIT)*, Tlemcen, 2015.

[28] T. Tantichanakul, O. Chailapakul and N. Tantavichet, “Gelled electrolytes for use in absorptive glass mat valve-regulated lead-acid (AGM VRLA) batteries working under 100% depth of discharge conditions,” *Journal of Power Sources,* vol. 196, no. 20, pp. 8764-8772, 2011.

[29] V. Gevorgian and D. Corbus, “Ramping Performance Analysis of the Kahuku Wind-Energy Battery Storage System,” National Renewable Energy Laboratory, Denver, 2013.

[30] A. A. Akhil, A. T. Murray and M. Yamane, “Kauai Island Utility Cooperative Energy Storage Study,” Sandia National Laboratories, Albuquerque, 2009.

[31] S. Rothgang, T. Baumhöfer, H. v. Hoek, T. Lange, R. W. D. Doncker and D. U. Sauer, “Modular battery design for reliable, flexible and multi-technology energy storage systems,” *Applied Energy,* vol. 137, pp. 931-937, 2015.

[32] A. Marongiu, M. Roscher and D. U. Sauer, “Influence of the vehicle-to-grid strategy on the aging behavior of lithium battery electric vehicles,” *Applied Energy,* vol. 137, pp. 899-912, 2015.

[33] R. Godina, E. Rodrigues, J. Matias and J. Catalão, “Smart electric vehicle charging scheduler for overloading prevention of an industry client power distribution transformer,” *Applied Energy,* vol. 178, p. 29–42, 2016.

[34] Y. Cui, C. Du, G. Yin, Y. Gao, L. Zhang, T. Guan, L. Yang and F. Wang, “Multi-stress factor model for cycle lifetime prediction of lithium ion batteries with shallow-depth discharge,” *Journal of Power Sources,* vol. 279, pp. 123-132, 2015.

[35] L. Gaillac and N. Pinsky, “Southern California Edison (SCE) energy storage efforts,” in *in Proc. Adv. Automotive Battery Conf., LLIBTA*, Orlando, 2012.

[36] P. Bernard and M. Lippert, “Chapter 14 - Nickel–Cadmium and Nickel–Metal Hydride Battery Energy Storage,” in *Electrochemical Energy Storage for Renewable Sources and Grid Balancing*, Amsterdam, Elsevier, 2015, pp. 223-251.

[37] BASF, “BASF to present new developments in NiMH batteries for grid energy storage applications at IRES 2013,” BASF, 2013. [Online]. Available: http://www.catalysts.basf.com/p02/USWeb-Internet/en_GB/content/microsites/catalysts/news/news196. [Accessed 02 12 2015].

[38] L. Balza, C. Gischler, N. Janson, S. Miller and G. Servetti, “Potential for Energy Storage in Combination with Renewable Energy in Latin America and the Caribbean,” Inter-American Development Bank, 2014.

[39] M. Thele, O. Bohlen, D. U. Sauer and E. Karden, “Development of a voltage-behavior model for NiMH batteries using an impedance-based modeling concept,” *Journal of Power Sources,* vol. 175, no. 1, pp. 635-643, 2008.

[40] E. Wesoff, “Kawasaki Heavy Revving Up on Energy Storage,” Greentech Media, 05 2010. [Online]. Available: http://www.greentechmedia.com/articles/read/kawasaki-heavy-goes-large-on-energy-storage. [Accessed 02 12 2015].

[41] B. E. Conway, Electrochemical supercapacitors: scientific fundamentals and technological applications, New York: Springer, 2009.

[42] A. Jossen, “Fundamentals of battery dynamics,” *Journal of Power Sources,* vol. 154, no. 2, pp. 530-538, 2006.

[43] H. Chan, “A new battery model for use with battery energy storage systems and electric vehicles power systems,” in *IEEE Power Engineering Society Winter Meeting, 2000.*, 2000.

[44] M. G. Jayne and C. Morgan, “The modelling a lead acid batteries for electric vehicle applications,” in *32nd International Power Sources Symposium*, Cherry HilL, 1986.

[45] I. Papic, “Simulation model for discharging a lead-acid battery energy storage system for load leveling,” *IEEE Transactions on Energy Conversion,* vol. 21, no. 2, pp. 608-615, 2006.

[46] M. Chen and G. Rincon-Mora, “Accurate electrical battery model capable of predicting runtime and I-V performance,” *IEEE Transactions on Energy Conversion,* vol. 21, no. 2, pp. 504-511, 2006.

[47] Z. Salameh, M. Casacca and W. A. Lynch, "A mathematical model for lead-acid batteries," *IEEE Transactions on Energy Conversion,* vol. 7, no. 1, pp. 93-98, 1992.

[48] S. Buller, M. Thele, R. De Doncker and E. Karden, "Impedance-based simulation models of supercapacitors and Li-ion batteries for power electronic applications," in *38th IAS Annual Meeting. Conference Record of the Industry Applications Conference, 2003.*, 2003.

[49] I. Sadli, P. Thounthong, J.-P. Martin, S. Raël and B. Davat, "Behaviour of a PEMFC supplying a low voltage static converter," *Journal of Power Sources,* vol. 156, no. 1, pp. 119-125, 2006.

[50] O. Bohlen, S. Buller, R. De Doncker, M. Gelbke and R. Naumann, "Impedance based battery diagnosis for automotive applications," in *IEEE 35th Annual Power Electronics Specialists Conference, 2004.*, Aachen, Germany, 2004.

[51] D. Fan and R. E. White, "A Mathematical Model of a Sealed Nickel-Cadmium Battery," *Journal of the Electrochemical Society,* vol. 138, no. 1, pp. 17-25, 1991.

[52] E. Kuhn, C. Forgez, P. Lagonotte and G. Friedrich, "Modelling Ni-mH battery using Cauer and Foster structures," *Journal of Power Sources,* vol. 158, no. 2, pp. 1490-1497, 2006.

[53] G. Sperandio, C. Nascimento and G. Adabo, "Modeling and simulation of nickel-cadmium batteries during discharge," in *2011 IEEE Aerospace Conference*, Big Sky, MT, 2011.

[54] B. Schweighofer, K. Raab and G. Brasseur, "Modeling of high power automotive batteries by the use of an automated test system," *IEEE Transactions on Instrumentation and Measurement,* vol. 52, no. 4, pp. 1087-1091, 2003.

[55] W. Guoliang, L. Rengui, Z. Chunbo and C. C.C., "State of charge Estimation for NiMH Battery based on electromotive force method," in *2008. VPPC '08. IEEE Vehicle Power and Propulsion Conference*, Harbin, 2008.

[56] Y.-C. Hsieh, T.-D. Lin, R.-J. Chen and H.-Y. Lin, "Electric circuit modelling for lithium-ion batteries by intermittent discharging," *IET Power Electronics,* vol. 7, no. 10, pp. 2672-2677, 2014.

[57] P. D. Lund, J. Lindgren, J. Mikkola and J. Salpakari, "Review of energy system flexibility measures to enable high levels of variable renewable electricity," *Renewable and Sustainable Energy Reviews,* vol. 45, pp. 785-807, 2015.

[58] C.-J. Zhan, X. Wu, S. Kromlidis, V. Ramachandaramurthy, M. Barnes, N. Jenkins and A. Ruddell, "Two electrical models of the lead-acid battery used in a dynamic voltage restorer," *IEE Proceedings on Generation, Transmission and Distribution,* vol. 150, no. 2, pp. 175-182, 2003.

[59] M. Ceraolo, "New dynamical models of lead-acid batteries," *IEEE Transactions on Power Systems,* vol. 15, no. 4, pp. 1184-1190, 2000.

[60] S. Barsali and M. Ceraolo, "Dynamical Models of Lead-Acid Batteries: Implementation Issues," *IEEE Transactions on Energy Conversion,* vol. 17, no. 1, pp. 16-23, 2002.

[61] X. Luo, J. Wang, M. Dooner and J. Clarke, "Overview of current development in electrical energy storage technologies and the application potential in power system operation," *Applied Energy,* vol. 137, pp. 511-536, 2015.

[62] J. B. Copetti, E. Lorenzo and F. Chenlo, "A general battery model for PV system simulation," *Progress in Photovoltaics: Research and Applications,* vol. 1, no. 4, p. 283–292, 1993.

[63] J. Copetti and F. Chenlo, "Lead/acid batteries for photovoltaic applications. Test results and modeling," *Journal of Power Sources,* vol. 47, no. 1, pp. 109-118, 1994.

[64] D. U. Sauer and H. Wenzl, "Comparison of different approaches for lifetime prediction of electrochemical systems—Using lead-acid batteries as example," *Journal of Power Sources,* vol. 176, no. 2, pp. 534-546, 2008.

[65] J. Schiffer, D. U. Sauer, H. Bindner, T. Cronin, P. Lundsager and R. Kaiser, "Model prediction for ranking lead-acid batteries according to expected lifetime in renewable energy systems and autonomous power-supply systems," *Journal of Power Sources,* vol. 168, no. 1, pp. 66-78, 2007.

[66] J. Guo, Z. Li and M. Pecht, "A Bayesian approach for Li-Ion battery capacity fade modeling and cycles to failure prognostics," *Journal of Power Sources,* vol. 281, pp. 173-184, 2015.

[67] P. Munoz-Condes, M. Gomez-Parra, C. Sancho, M. San Andres, F. Gonzalez-Fernandez, J. Carpio and R. Guirado, "On Condition Maintenance Based on the Impedance Measurement for Traction Batteries: Development and Industrial Implementation," *IEEE Transactions on Industrial Electronics,* vol. 60, no. 7, pp. 2750-2759, 2013.

[68] Y. Barsukov and J. Qian, Battery Power Management for Portable Devices, Norwood, MA: Artech House Power Engineering, 2013.

[69] T. Guena and P. Leblanc, "How Depth of Discharge Affects the Cycle Life of Lithium-Metal-Polymer Batteries," in *28th Annual International Telecommunications Energy Conference, 2006. INTELEC '06.*, Providence, RI, 2006.

[70] H. Bindner, T. Cronin, P. Lundsager, J. F. Manwell, U. Abdulwahid and I. Baring-Gould, "Lifetime Modelling of Lead Acid Batteries," Risø National Laboratory, Roskilde, 2005.

[71] D. A. Wetz, B. Shrestha, S. T. Donahue, D. N. Wong, M. J. Martin and J. Heinzel, "Capacity Fade of 26650 Lithium-Ion Phosphate Batteries Considered for Use Within a Pulsed-Power System's Prime Power Supply," *EEE Transactions on Plasma Science,* vol. 45, no. 5, pp. 1448-1455, 2015.

[72] T. Hund, N. Clark and W. Baca, "Ultrabattery Test Results for Utility Cycling Applications," in *The 18 International Seminar on Double Layer Capacitors and Hybrid Energy Storage Devices*, 2008.

[73] H. Nakajima, T. Honma, K. Midorikawa, Y. Akasaka, S. Shibata, H. Yoshida, K. Hashimoto, Y. Ogino, W. Tezuka, M. Miura, J. Furukawa, L. T. Lam and S. Sugata, “Development of UltraBattery,” *Furukawa Review,* vol. 43, pp. 2-9, 2013.

[74] D. Christian, “Développement d'outils pour l'analyse des systèmes hybrides photovoltaïque-diesel,” Ecole nationale supérieure des mines de Paris, Paris, 1999.

Unit Technology		Unit Fuel	Number of Generating Units	Installed Capacity [MW]
Conventional	Steam	Fuel-Oil	7	198
	Combined-cycle gas turbine (CCGT)	Diesel	1	132
	Open-cycle gas turbine (OCGT)	Diesel	11	290
	Internal Combustion Engine (ICE)	Fuel-Oil	6	145
RES	Wind	-	32	194
	PV	-	-	96
	Small Hydro	-	1	0.3
	Geothermal	-	-	-
	Biogas		2	0.4
TOTAL				1055.7
Energy Consumption 2014 [MWh]		2,983,491		
Peak Demand 2014 [MW]		597.5		
Minimum Demand 2014 [MW]		170.2		

Table. 1 – Crete power system generation data

Unit Technology		Unit Fuel	Number of Generating Units	Installed Capacity [MW]
ICE		Heavy Fuel-Oil	8	98
RES	Wind	-	10	9
	PV	-	-	-
	Small Hydro	-	7	5
	Geothermal	-	5	24
	Biogas			
TOTAL				136
Energy Consumption [MWh] (2014)		415,549		
Peak Demand [MW] (2014)		68.17		
Minimum Demand [MW] (2014)		29.35		

Table. 2 – São Miguel power system generation data

Type	Cycles (80%)	Charge Time (h)	Discharge Month (%)	Cost ($/KWh)	Voltage (V)	Peak Drain (C)	Specific Energy (Wh/kg)	Specific Power (W/kg)	Rated Capacity (mAh)	Nominal C-Rate	Max C-Rate
Li-ion	500–1000	2-4	10	24	4.2	2	90–190	500–2000	5300	2C	20C
NiMH	300–500	2-4	30	18.5	1.25	5	45–80	200–1500	2300	0.5C-1C	1C
NiCd	1500	1	20	7.5	1.25	20	40–65	100–175	2800	0.1C	3C
PbA	200–2000	8-16	5	8.5	2	5	20–40	75–415	2000	0.2C	3.3C

Table 3 – Main features of the electrochemical batteries under review.

	Lithium-ion	NiMH	NiCd	PbA
SOC	34.09	33.15	33.99	30.12
SEI	92.34	86.82	95.10	27.15
DRI	97.83	96.98	100	82.31

Table 4 – Merit figures outcomes: Azores.

	Lithium-ion	NiMH	NiCd	PbA
SOC	91.01	93.78	96.43	8.98
SEI	11.20	16.15	22.05	3.91
DRI	19.03	19.08	45.87	13.11

Table 5 – Merit figures outcomes: Crete.

Cycles (80%)	200–2000
Charge Time (h)	8–16
Discharge Month (%)	5
Cost ($/ KWh)	8.5
Voltage (V)	2.085
Peak Drain (C)	5
Specific Energy (W h/kg)	20–40
Specific Power (W/kg)	75–415
Rated Capacity (mAh)	2000

Table 6 – PbA electrochemical battery main characteristics.

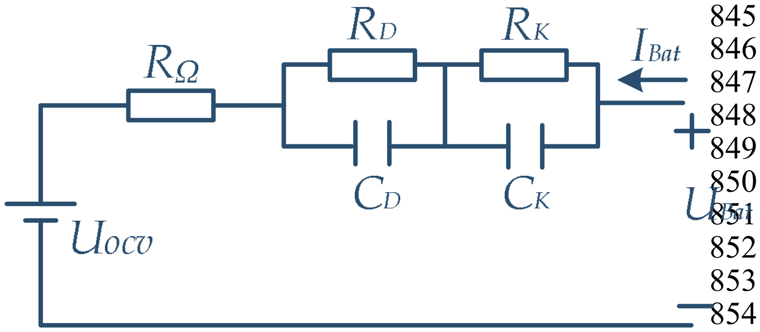

Fig. 1 – NiMH battery model

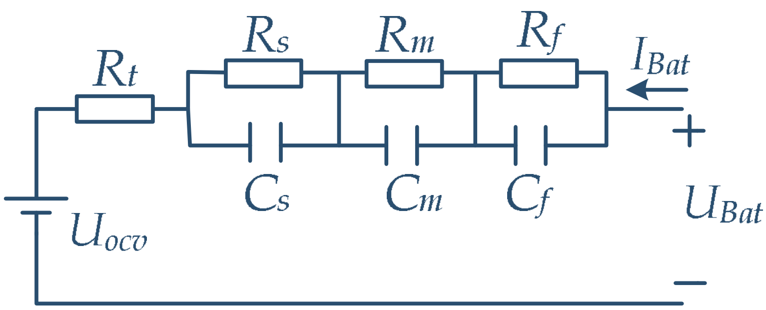

Fig. 2 – Li-ion battery model

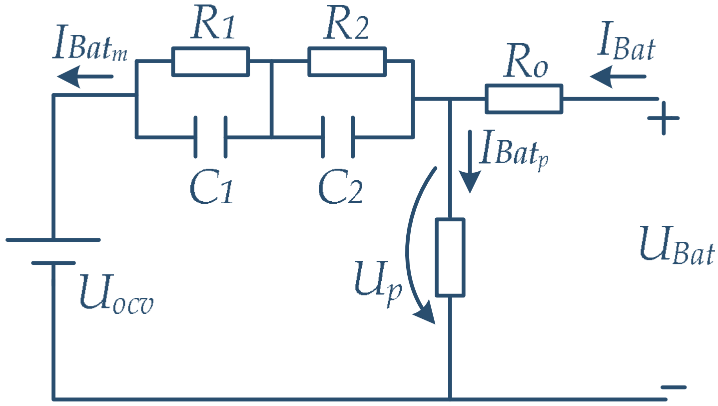

Fig. 3 – PbA battery equivalent network

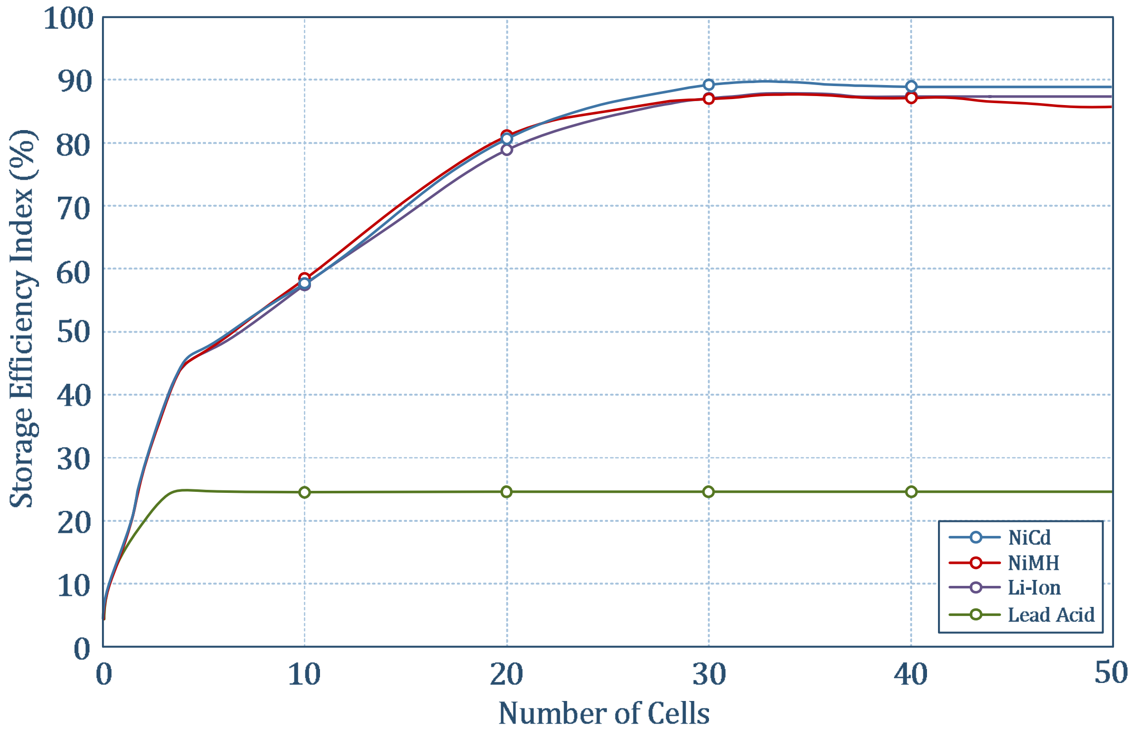

Figure 4 - São Miguel: SEI.

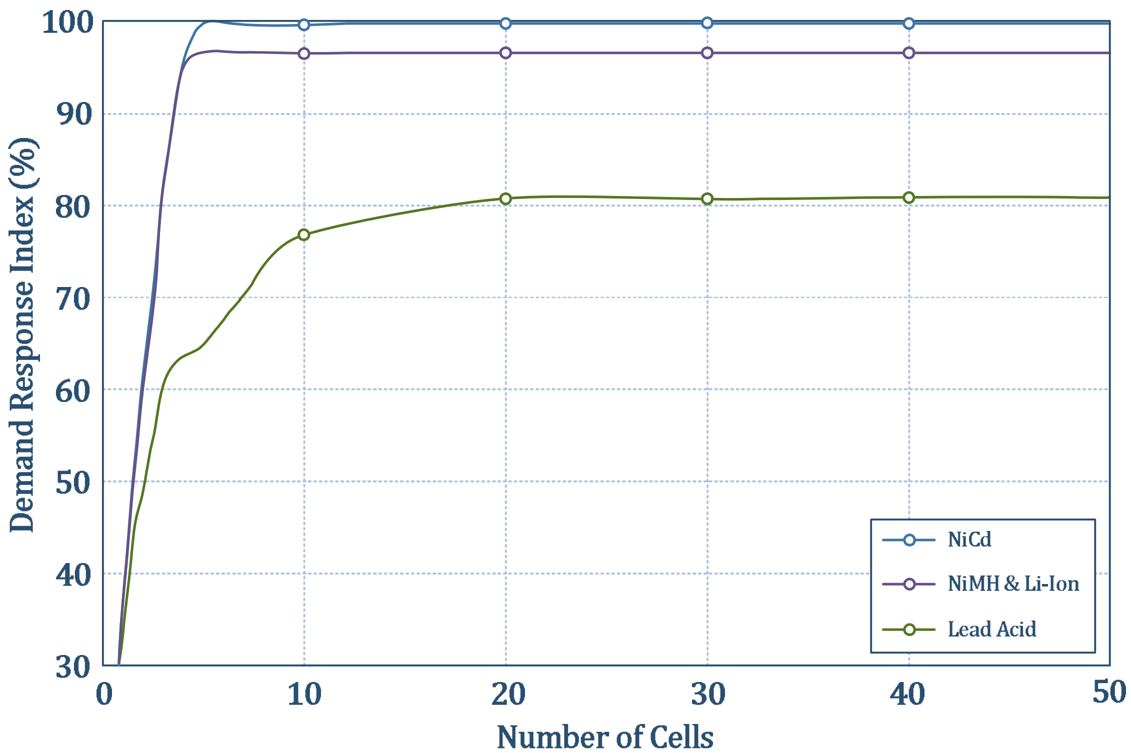

Figure 5 - São Miguel: DRI.

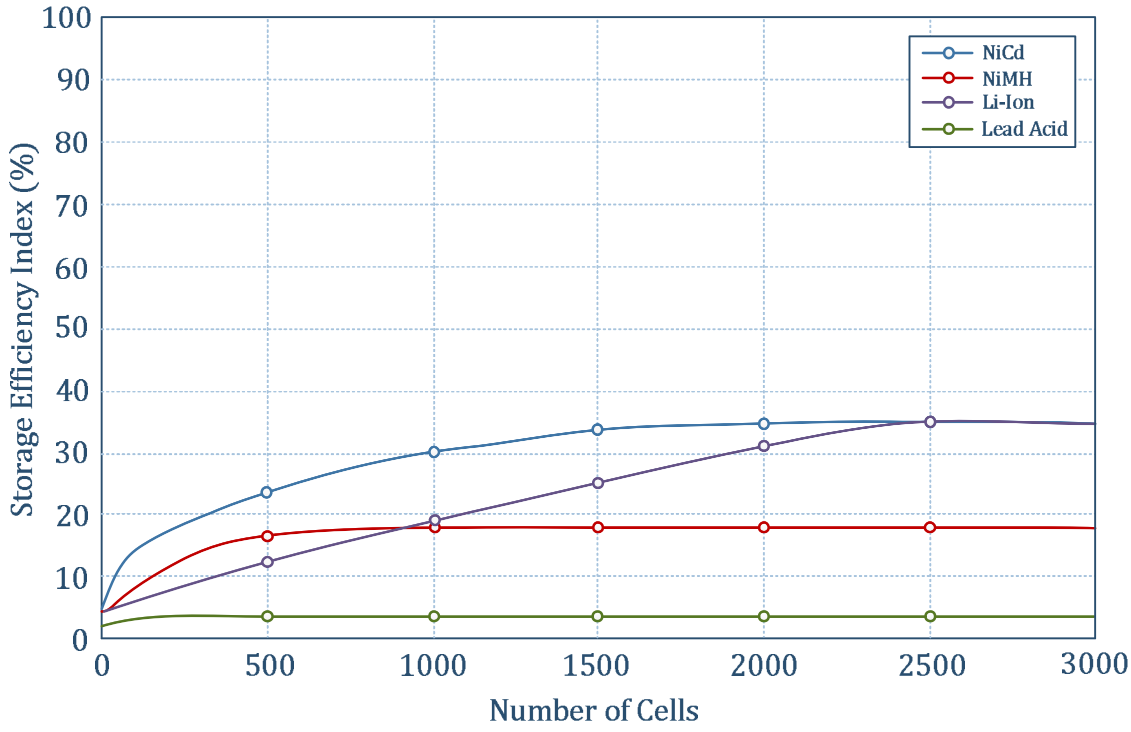

Figure 6 – Crete: SEI.

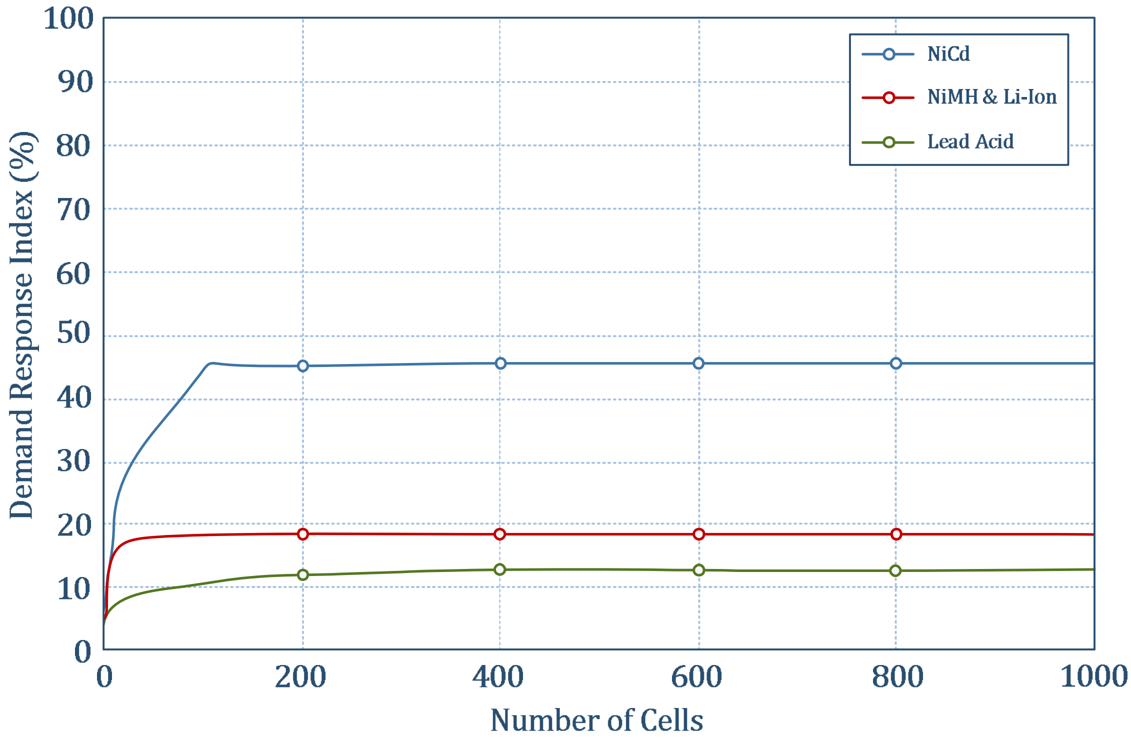

Figure 7 - Crete: DRI.

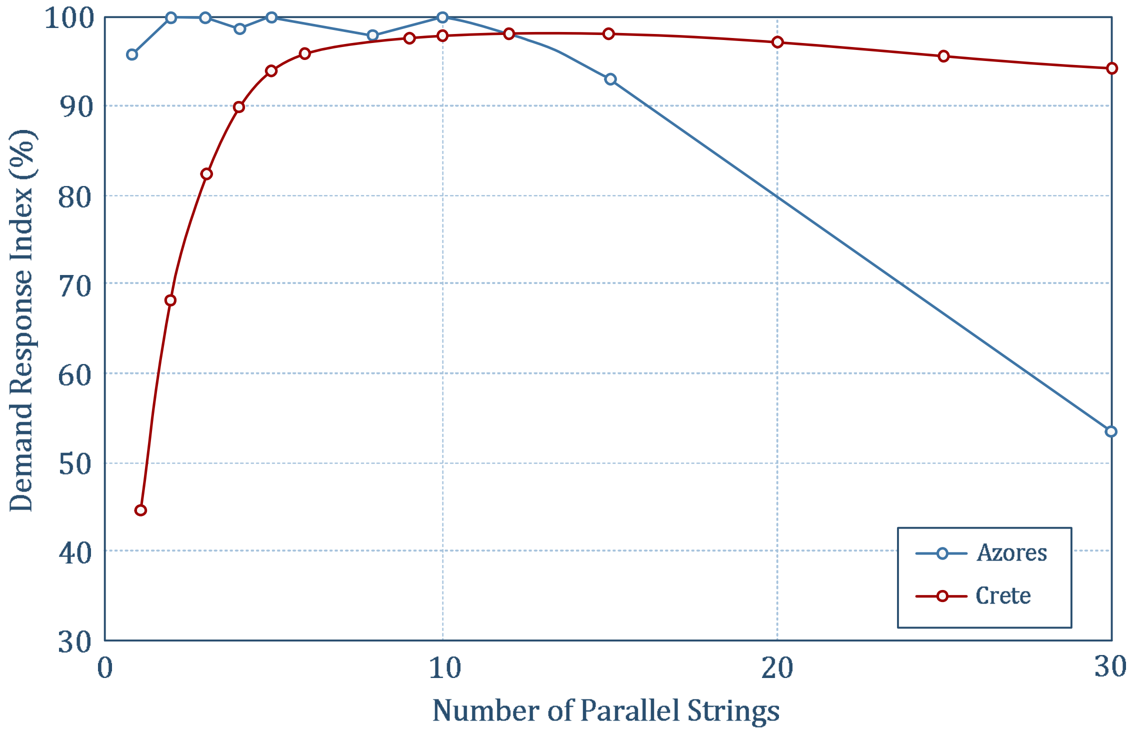

Figure 8 – Effect of the number of strings on DRI.

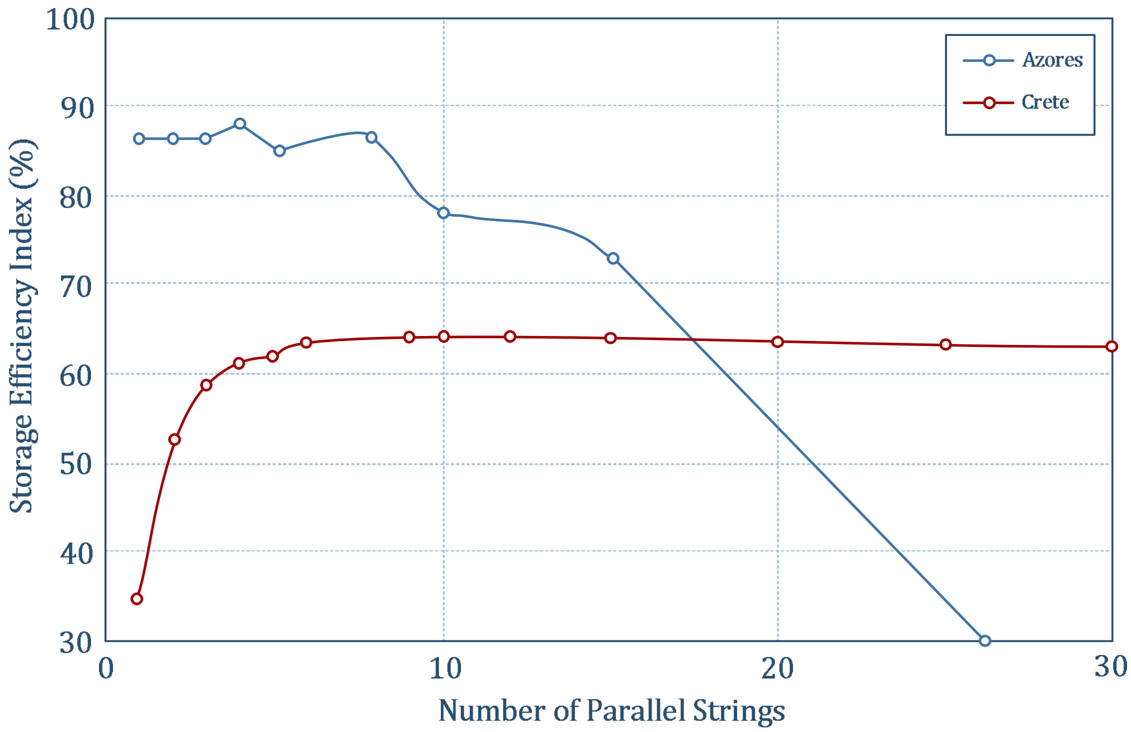

Figure 9 – Effect of the number of strings on SEI.

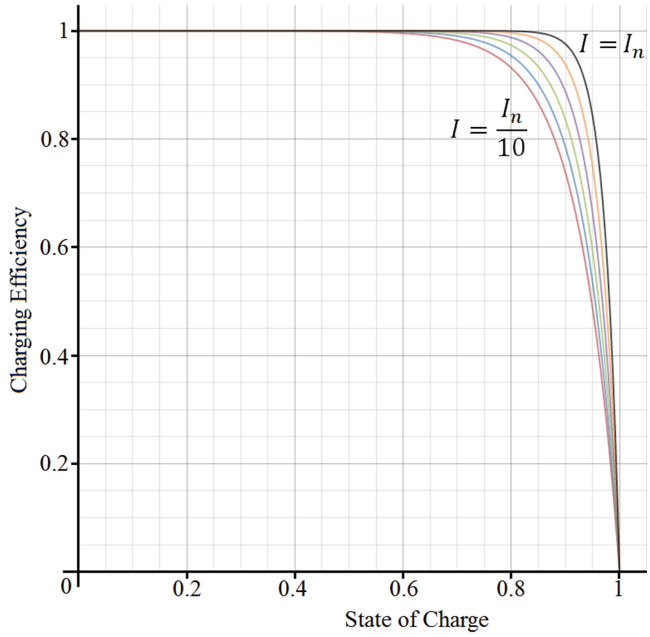

Figure 10 – Charging efficiency as function of SOC.

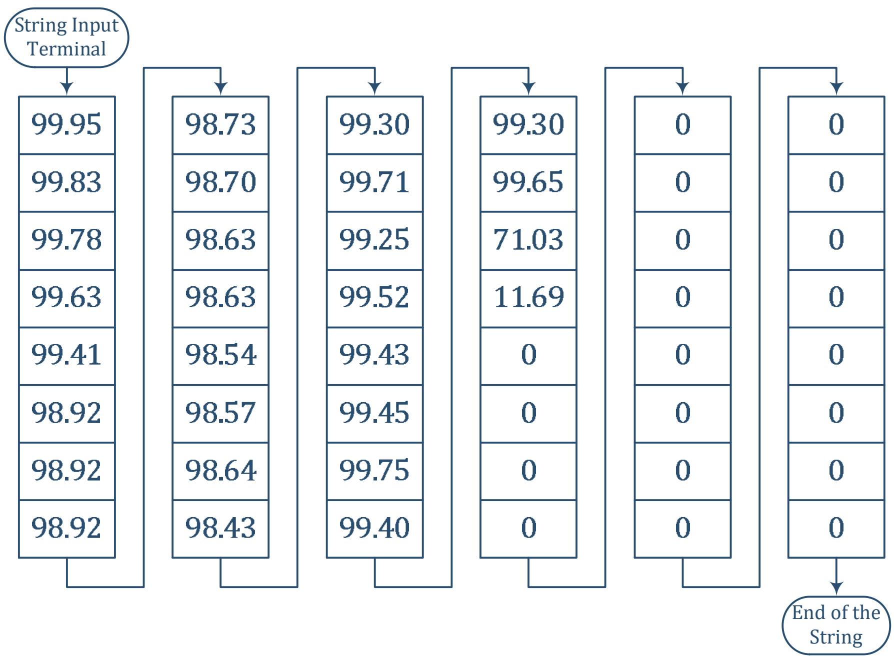

Figure 11 - Configuration in single string: SOC per cell.

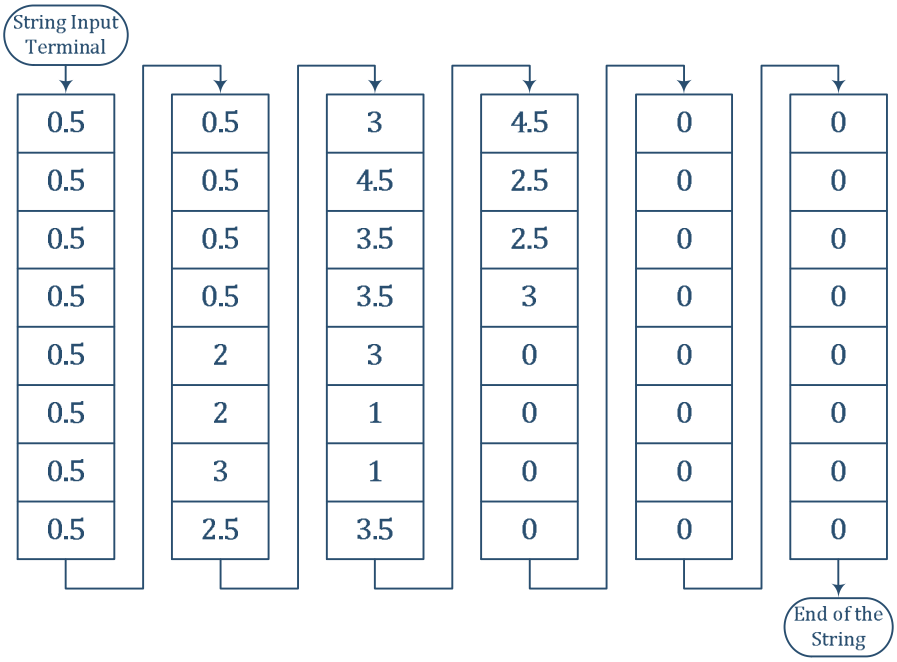

Figure 12 - Configuration in single string: Number of charging cycles.

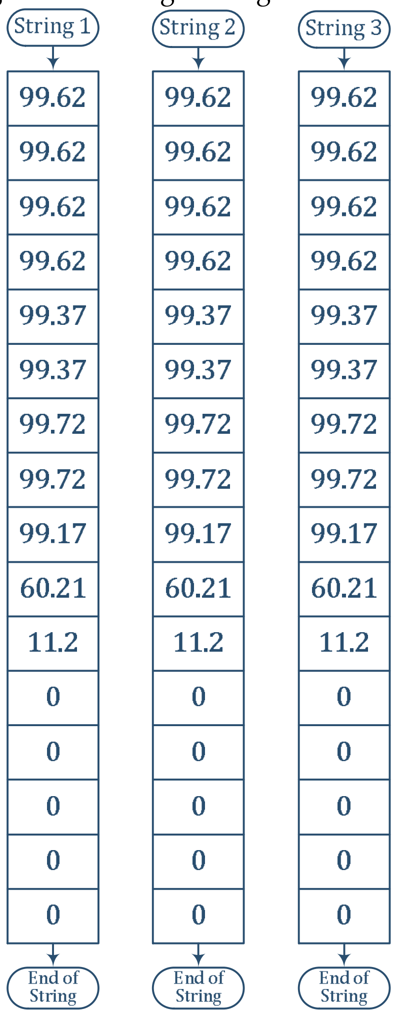

Figure 13 - Parallel configuration: SOC per cell.

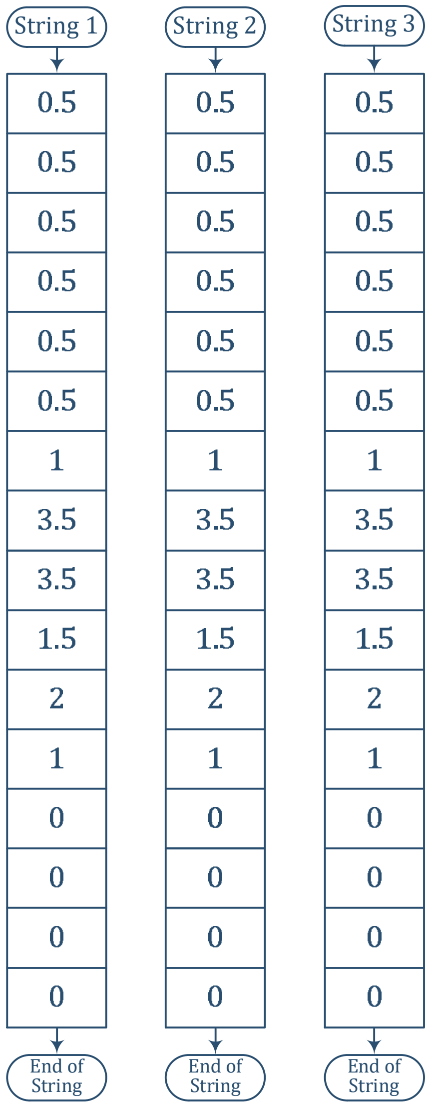

Figure 14 – Parallel configuration: Number of charging cycles.

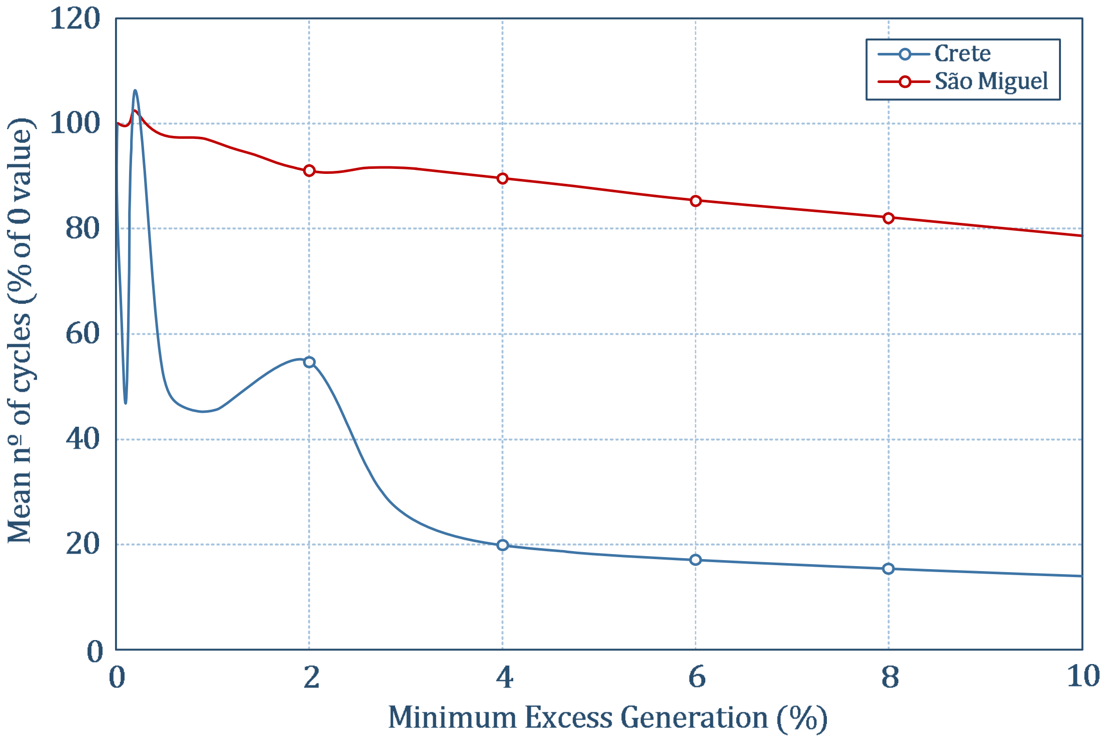

Figure 15- Average number of battery cycles to charging criterion.

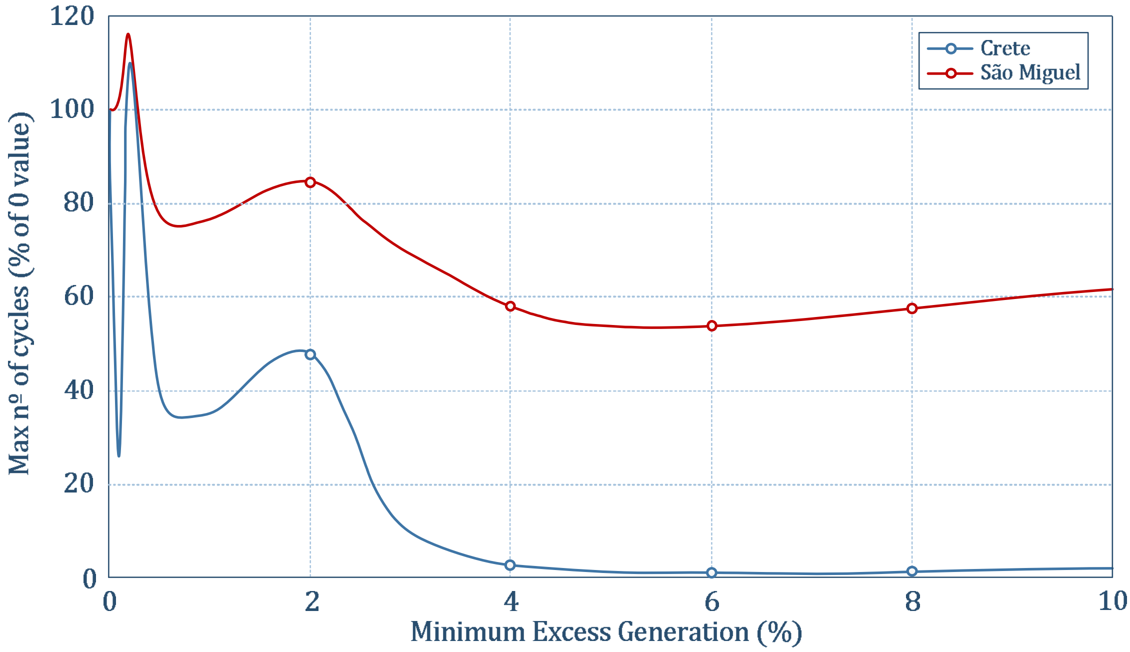

Figure 16 - Battery cycles maximum number to charging criterion.

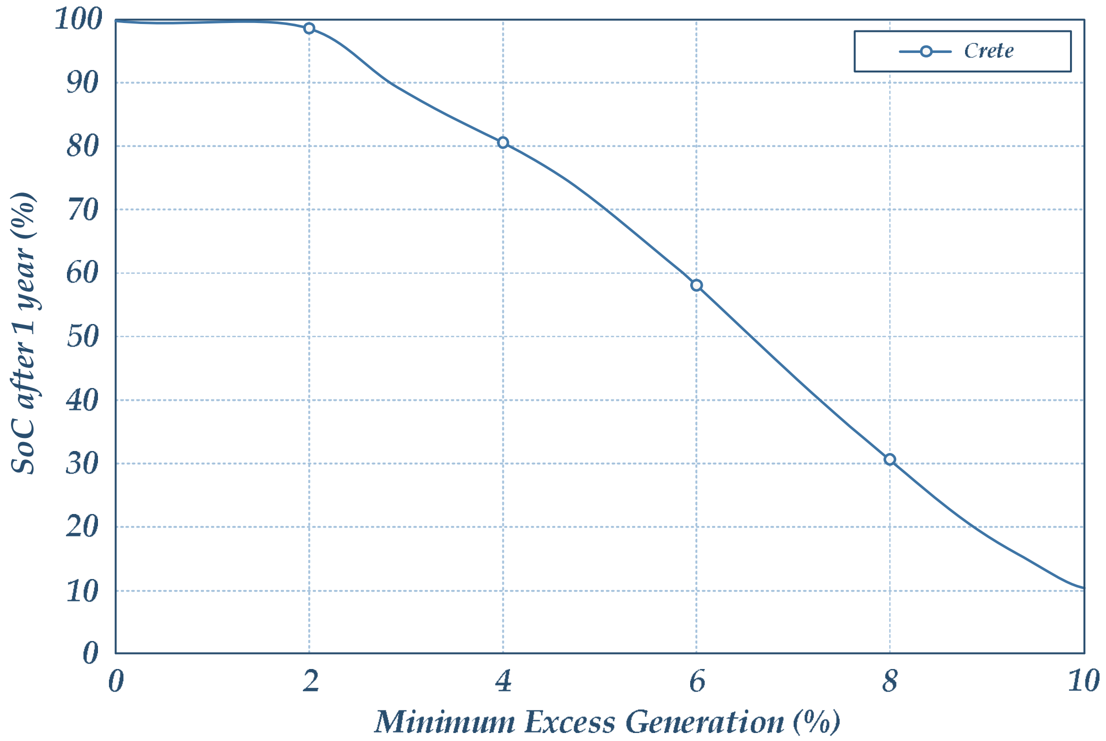

Figure 17 – SOC profile as function of the charging criterion.